Implementation of the Quasi-equilibrium Tropical Circulation Model 2 (QTCM2): Global simulations and convection sensitivity to free tropospheric moisture

Benjamin R. Lintner[1], Gilles Bellon[2], Adam H. Sobel[3,4,5], Daehyun Kim[3], J. David Neelin[6]

Submitted to Journal of Advances in Modeling Earth Systems

May 29, 2012

[1]*Department of Environmental Sciences, Rutgers, The State University of New Jersey, New Brunswick, NJ, USA*

[2] *Centre National de Recherches Météorologiques, Centre National de la Recherche Scientifique /Météo-France, Toulouse, France*

[3]*Department of Applied Physics and Applied Mathematics, Columbia University, New York, NY, USA*

[4]*Department of Earth and Environmental Sciences, Columbia University, New York, NY, USA*

[5]*Lamont-Doherty Earth Observatory, Columbia University, New York, NY, USA*

[6]*Department of Atmospheric and Oceanic Sciences and Institute of Geophysics and Planetary Physics, University of California Los Angeles, Los Angeles, CA, USA*

*Corresponding author: Benjamin R. Lintner, Department of Environmental Sciences, Rutgers, The State University of New Jersey, 14 College Farm Road, New Brunswick, NJ 08901-8551, USA

Email: lintner@envsci.rutgers.edu

Telephone: (732) 932-9800 ext. 6223

Abstract. The implementation of the Quasi-equilibrium Tropical Circulation Model 2 (QTCM2), an intermediate level complexity model, is described. Following the approach of Sobel and Neelin (2006), an explicit, prognostic atmospheric boundary layer (ABL) of fixed depth is added to a free troposphere (FT) containing one baroclinic and one barotropic mode. QTCM2 is shown to simulate reasonable climatologies of temperature, moisture, winds, and precipitation, albeit with only modest improvements relative to the predecessor single vertical mode version, QTCM1. The addition of an ABL increases the sharpness of horizontal precipitation and moisture gradients, and the separation of the moisture profile into ABL and FT components allows investigation into the separate roles of these two components in modulating deep convection. Model sensitivity to various convection parameters is explored, with contrasting precipitation responses often seen within the cores of convecting regions and along their margins.

1. Introduction

Quasi-equilibrium Tropical Circulation Models (QTCMs) are a family of intermediate level complexity models employing a Galerkin-like vertical discretization in which the primitive equations are projected onto a few prescribed, physically-based, vertical structure functions (Neelin and Zeng, 2000). For large-scale tropical motions, the term convective quasi-equilibrium (QE) refers to the idea that deep convection constrains the vertical structure of temperature and moisture to lie close to known statistical equilibrium profiles in convecting regions. Efficient equatorial wave dynamics communicates the temperature structure laterally throughout the Tropics. For a given temperature basis function and assuming hydrostatic balance, basis functions for velocity are constructed to be consistent with the implied vertical structures of baroclinic and barotropic pressure gradients. The first QTCM, hereafter QTCM1, comprises a single first baroclinic mode in temperature and barotropic and first baroclinic modes in momentum (Zeng et al. 2000).

In contrast to many other idealized models, QTCM1 retains nonlinearities inherent to the primitive equations and further incorporates parameterizations resembling those found in general circulation models (GCMs). For example, the radiative scheme implemented in QTCM1 was derived from a linearized radiative transfer scheme (Chou and Neelin 1996) and includes cloud-radiative feedbacks for different cloud types. Apart from QTCM1's computational efficiency, one of the more useful aspects of the model is the ease of diagnosis of tropical moist dynamics. Among the diverse phenomena previously studied with QTCM1 are: tropical land and ocean region precipitation climatology and variability (Zeng et al. 2000); remote tropical ENSO teleconnections (Chiang and Sobel 2002; Neelin and Su 2005; Lintner and Chiang 2007); global warming impacts on tropical precipitation (Neelin et al. 2003; Chou and Neelin 2004);

midlatitude transient effects on tropical precipitation variability (Lin et al. 2000); and theories for monsoon structure and spatial characteristics in current and past climates (Chou and Neelin 2003; Su and Neelin 2005). Moreover, the vertically-projected equations in QTCM1 have been used as a starting point for analytic solutions for tropical circulations under the weak temperature gradient approximation (Sobel and Bretherton 2000; Sobel et al. 2001); idealized models of Hadley and Walker circulations (Bretherton and Sobel 2002; Sobel et al. 2004; Burns et al. 2006); convectively coupled waves (Khouider and Majda 2006; Frierson 2007); interactions of inflow air mass characteristics with tropical deep convection (Lintner and Neelin 2007, 2008); and land-atmosphere coupling (Lintner et al. 2012). Such analytical solutions often suggest relationships that are not obvious from diagnostics alone and facilitate the development of additional diagnostics for more complex models.

While QTCM1 has yielded insights into a wide range of tropical phenomena, the limited vertical degrees of freedom in QTCM1 preclude consideration of some fundamental aspects of tropical climate. One obvious limitation of QTCM1 is its lack of an explicit atmospheric boundary layer (ABL) independent of the free troposphere (FT). To address this limitation, Sobel and Neelin (2006; hereafter SN06) developed a self-consistent, axisymmetric version of QTCM with separate thermodynamic and momentum equations for the ABL and FT. SN06 used their two-level QTCM, or QTCM2, to examine how thermodynamic and momentum controls contribute to the intensity and meridional extent of Intertropical Convergence Zones (ITCZs). They found that inclusion of an ABL in the axisymmetric configuration enhances both the amplitude and sharpness of ITCZs, consistent with boundary layer convergence acting as a forcing on the free troposphere (FT) (Lindzen and Nigam 1987; Back and Bretherton 2009). Bellon and Sobel (2010) used the axisymmetric model of SN06 to investigate equatorial

symmetry-breaking mechanisms and the occurrence of multiple equilibria for the Hadley circulation. This axisymmetric model was further used to study mechanisms of the monsoon intraseasonal oscillation (Bellon and Sobel 2008a, 2008b), as well as its coupling with oceanic and continental surfaces (Bellon et al. 2008; Bellon 2011).

The present study extends the axisymmetric QTCM2 of SN06 to a non-axisymmetric "2.5D" configuration with realistic boundary conditions. Following a brief discussion of the model's implementation (Section 2), we present an overview of QTCM2-simulated climatologies (Section 3). Section 4 highlights some aspects of QTCM2 sensitivity: in particular, we directly illustrate how independent ABL and FT thermodynamics and dynamics, the principal difference vis-à-vis QTCM1, impact precipitation simulation. We further demonstrate how the use of revised vertical structure functions and a modified convection scheme alter simulated precipitation.

Beyond the model configuration sensitivity analyses in Section 4, we also investigate some aspects of convective sensitivity to FT moisture (Section 5). While observational and cloud system resolving model studies indicate that moist convection is sensitive to FT moisture (Parsons et al. 2000; Tompkins 2001; Grabowski and Moncrieff 2004; Bretherton et al. 2004; Sherwood et al. 2004; Derbyshire et al. 2004), global climate models (GCMs) often underestimate or otherwise fail to reflect this sensitivity (Biasutti et al. 2006; Dai 2006). The lack of sensitivity may stem from underestimation of entrainment and rain re-evaporation, so models produce deep convection too readily (Kuang and Bretherton 2007; Del Genio 2011). At the same time, GCM studies provide evidence that the entrainment rate or other parameters impacting this convective moisture sensitivity have a substantial impact on many phenomena including intraseasonal variability such as the Madden Julian Oscillation (MJO) (Grabowski

2006; Kim et al. 2011; Hannah and Maloney 2011), and that deficiencies in model representation of feedbacks between moisture, deep convection, and circulation may ultimately limit the ability of GCMs to simulate multiscale convective organization (Holloway and Neelin 2010), particularly on intraseasonal scales. Although the analysis presented in Section 5 is cursory, we believe it illustrates QTCM2's utility as a tool for addressing some important features of convective sensitivity to FT moisture.

2. Model implementation

The implementation of the non-axisymmetric QTCM2 with realistic boundary conditions closely follows the implementation of the axisymmetric version described in SN06. Relative to QTCM1, these modifications fall into one of three categories: (i) *model physics*, associated with the added vertical degree of freedom; (ii) *model parameterization schemes*, revised as a result of separating the ABL and FT basis functions (but which are updated within the same overall physical framework); and (iii) *model parameters*, revised as a result of the updated vertical basis functions. We also note that several errors in the base code for QTCM1 (specifically, version 2.3) have been corrected, although the impacts of these on simulations performed with existing model versions are small. Below we highlight key features of QTCM2, noting specifically where the implementation diverges from either SN06 or the QTCM1v2.3 base code. The reader is referred to Appendix A for a more detailed review of the mathematical basis of QTCM2. QTCM2 source code and documentation can be found at: http://www.atmos.ucla.edu/~csi/QTCM/qtcm.html.

2.1 Momentum equations formulated in vorticity-divergence form

The major structural difference in the full non-axisymmetric implementation involves the ABL and barotropic velocity fields. (We use the term "barotropic" loosely here to refer to the vertically uniform component of the FT velocity; because the ABL velocity differs from that component, it is not truly barotropic.) For the axisymmetric version of SN06, the column-integrated meridional momentum, a linear combination of the ABL and barotropic meridional winds, is identically zero, because of the axisymmetric continuity equation and the latitudinal boundary conditions. This allowed the use of meridional momentum budgets in the ABL and the FT to compute the gradient of surface geopotential and either the ABL or the barotropic meridional wind. In the present non-axisymmetric implementation, this is not the case; rather, we use the vorticity-divergence (vort-div) form of the barotropic momentum equations. (The baroclinic momentum equations are solved in component form.) Consider the time-tendency of the (horizontal) barotropic momentum in the FT:

$$\partial_t \mathbf{v_0} = \mathbf{F_{v0}} \tag{1}$$

where $\mathbf{F_{v0}}$ represents sum of all barotropic momentum tendencies. Expanding the wind in divergent and rotational components $\mathbf{v_0} = \mathbf{v}_\chi + \mathbf{v}_\psi = \nabla\phi + \nabla \times \psi\hat{\mathbf{k}}$, with Φ the velocity potential and ψ the streamfunction, and evaluating the curl and divergence of Equation (1) gives respectively:

$$\nabla^2 \partial_t(\phi, \psi) = (\nabla \cdot \mathbf{F_{v0}}, \hat{\mathbf{k}} \cdot \nabla \times \mathbf{F_{v0}}) \tag{2}$$

Equation (2) is of the form of a Poisson equation in the time-tendencies of the scalar velocity potentials ϕ and ψ. Formally, an analogous equation applies to the ABL, although the divergent ABL and FT barotropic winds are related through mass conservation as in equation (A13). Fast-Fourier Transform Poisson solvers are applied to equation (2) as well as the ABL

158 streamfunction equation to obtain the time-tendencies of Φ and ψ, which are updated and then
159 used to obtain the velocity fields.
160
161 **2.2 Vertical structure coefficients**
162 The implementation of QTCM2 employs revised temperature, moisture, and first baroclinic
163 momentum basis functions, $a_1(p)$, $b_1(p)$, and $V_1(p)$ in the FT portion of the domain as
164 described in Holloway and Neelin (2007, 2009) (see Fig. 1). Relative to the vertical profiles
165 assumed in QTCM1, the revised temperature profile $a_1(p)$ includes a partial representation of
166 the convective cold top, with the relative weighting decreasing in the upper troposphere above
167 ~250 mb, while the revised moisture profile $b_1(p)$ implies lower values in the lower FT.
168 Differences in the simulation of the cold top in aquaplanet GCMs appear to contribute to
169 intermodel differences in ITCZ structure and ITCZ regime transitions (Oueslati and Bellon
170 2012a). In the ABL, the basis functions are assumed to be vertically uniform. Values of
171 coefficients precomputed from these basis functions are summarized in Table 1.
172 As discussed in SN06, gross stratifications are computed for both the FT barotropic and
173 baroclinic modes; these are of the general form:

174
$$\begin{aligned} M_{si} &= M_{sri} + M_{spi} T_1 \\ M_{qi} &= M_{qri} + M_{qpi} q_1 \end{aligned} \tag{3}$$

175 where the index i is either 0 or 1. With the exception of the baroclinic dry static stability, M_{s1},
176 these are computed consistently from the vertical profiles. Allowing M_{s1} to vary with
177 temperature, as in (3), renders the model unstable. Based on test runs to assess model stability,
178 M_{s1} is set to a constant value of 3.27 K, or approximately 1K higher than the reference value
179 M_{sr1}.

180

181 **2.3 Clouds, radiation, and surface fluxes**

182 Cloud prediction is performed as in QTCM1, by assuming four cloud types (deep convective,
183 cirrostratus, cirrocumulus, and stratus) with prescribed vertical structure. Shortwave and
184 longwave radiative transfer coefficients are precomputed using the scheme of Chou and Neelin
185 (1996) using the FT and ABL temperature and moisture basis functions in Fig. 1. QTCM2 uses
186 the SLAND1 land surface model as described in Zeng et al. (2000). While QTCM1 estimates
187 surface winds through a pseudo boundary layer, QTCM2 uses the boundary layer winds directly
188 to estimate drag coefficients for surface fluxes.

189

190 **2.4 Deep and shallow convection**

191 The deep convection scheme is identical to SN06, except a nonlinear scheme (as in QTCM1) is
192 used to calculate the convective moisture profile using the saturation moisture dependence on
193 temperature. A shallow convection parameterization is invoked when a quantity approximating
194 convective available potential energy (CAPE) is negative. Shallow convection uses the
195 relaxation scheme described in Neggers et al. (2007), with ABL convective heating, Qc_b, and
196 drying, Qq_b, given by:

197
$$\begin{matrix} Qc_b \\ Qq_b \end{matrix} = \begin{cases} \frac{T_{1c}^{sh} - s_b}{\tau_{sh}} \\ \frac{q_{1c}^{sh} - q_b}{\tau_{sh}} \end{cases} \qquad (4)$$

198 By definition, the net shallow convective heating and drying integrated over the entire depth of
199 the troposphere have zero integral. Thus, in the FT, shallow convective warming and drying,
200 Qc_f and Qq_f, are given by $(Qc_f, Qq_f) = -\frac{\Delta p_b}{\Delta p_f}(Qc_b, Qq_b)$. Here, the shallow convective

reference temperature and moisture values T_{1c}^{sh} and q_{1c}^{sh} are given by the values of dry static energy and moisture just above the boundary layer:

$$\begin{matrix} T_{1c}^{sh} \\ q_{1c}^{sh} \end{matrix} = \begin{cases} s_{re} + a_{1e} T_1 \\ q_{re} + b_{1e} q_1 \end{cases} \tag{5}$$

where s_{re} and q_{re} are reference values of dry static energy and specific humidity just above the ABL. As Neggers et al. (2007) note, the shallow convective adjustment timescale τ_{sh} can be related to the mixed layer depth z_b and the shallow cumulus mass flux m_b^{sh}, i.e., $\tau_{sh} \sim \frac{z_b}{m_b^{sh}}$, which is of order 10^5 s. Following Neggers et al. (2006), we implement a variable τ_{sh} by estimating the gridpoint convective velocity scale w^*, which is related to the surface buoyancy flux and can be expressed in terms of surface sensible and latent heating as described in Cuijpers and Bechtold (1995).

2.5 Numerics

We consider model simulations performed at both a fine resolution (1.40625° x 1°) and the coarse (5.625° x 3.75°) used as the default in QTCM1, with the model domain spanning 78.75°S-78.75°N. Fourier filtering is applied to prognostic variables to damp small-scale features for latitudes poleward of 45°. The prognostic equations are finite differenced on an Arakawa-C grid. Time tendencies of each prognostic variable are stored as arrays, and updates are performed simultaneously for all prognostic variables using a simple first order scheme, using a 10 minute timestep. Diffusion coefficients are set to values 60% higher than assumed in QTCM1 for added stability. On a Sun Fire workstation, one year of simulation at the low resolution can be executed in under 2 minutes wall-clock time.

Several switches are embedded in the code to facilitate implementation of different configurations of the model (see Section 4). For example, QTCM2 can be run in a "pseudo-QTCM1" configuration by slaving the FT and ABL thermodynamic and momentum equations; it is possible to run with slaved thermodynamics, slaved momentum, or both. Additional switches allow QTCM2 to be run with a QTCM1-like deep convection scheme and the original parameter set.

3. Baseline QTCM2 climatologies for DJF

Here we present a brief overview of the baseline climatologies of temperature, moisture, winds, and precipitation as simulated by QTCM2, focusing for simplicity on December-January-February (DJF). In what follows, we consider both the high- and low-resolution QTCM2 simulations. For temperature, moisture, and winds, we primarily focus on the ABL, as this represents, roughly-speaking, the added degree of freedom relative to QTCM1. Further discussion of precipitation appears in Sections 4 and 5. For comparison, we show comparable NCEP Reanalysis 2 (Kanamitsu et al. 2002) temperature, moisture, and wind fields and Climate Prediction Center Merged Analysis of Precipitation (CMAP; Xie and Arkin 1997) precipitation.

Relative to the NCEP Reanalysis 2m DJF surface air temperatures (Fig. 2a), QTCM2 surface air temperatures over the tropical oceans are generally low in the low resolution simulation (Fig. 2c) especially in the eastern Pacific, while in the high resolution simulation (Fig. 2b), the surface air temperature is too zonal in the southern Hemisphere. QTCM2-simulated DJF temperatures averaged over the depth of the troposphere (not shown) are more zonally-uniform than the surface air temperatures, as expected, although the band of warmest tropospheric mean temperatures in the deep tropics is somewhat too narrow. A cool bias in vertically-averaged

245 temperature was noted in the axisymmetric simulations of Bellon and Sobel (2010) and is also
246 evident in QTCM1 (not shown).

247 Comparing reanalysis to simulated moisture (Fig. 3), DJF near-surface specific humidity in
248 QTCM2 at either resolution is pervasively low over much of the tropical ocean. This also holds
249 for some land regions, although subtropical deserts in both hemispheres are too moist. Despite
250 the tendency for too dry conditions over tropical oceans, the gross spatial distribution of near
251 surface moisture in QTCM2 compares well to NCEP, e.g., the maximum DJF ABL moisture
252 occurs just to the north of Australia. Also, we note the impact of increased spatial resolution,
253 which somewhat mitigates the low bias over the ocean and high bias over the land. High values
254 of column water vapor (cwv; Fig. 4a) prevail in the low-latitudes of the SH, with peak values
255 exceeding 65 mm to the north of Australia and smaller maxima off the west coast of Africa and
256 over southeastern South America. Overall, cwv as simulated by the baseline QTCM2 is high-
257 biased near regions of intense tropical deep convection, especially at high resolution, although
258 cwv can be tuned through the convection scheme or other parameters such as the moisture
259 stratification.

260 The DJF boundary layer winds (Fig. 5; vectors) as simulated by QTCM2 are broadly
261 consistent with the leading features in the reanalysis, although the winds for the low resolution
262 simulation (Fig. 5c) are more zonal in the eastern Pacific and Atlantic. Also, only the high
263 resolution simulation captures the "roaring 40s" westerlies in the SH. At 200 mb, both the high
264 and low resolution QTCM2 configurations simulate easterlies over the deep Tropics (Fig. 5b;
265 filled contours), with localized centers near tropical continents. In the NH midlatitudes, westerly
266 wind maxima are found over the mid-East and in jet regions east of Japan and along the eastern
267 coastline of North America. However, the jet axes tilt unrealistically toward the southeast. The

upper tropospheric meridional winds (not shown) tend to be somewhat larger than observed, and for both the zonal and meridional components, the values are larger than simulated by QTCM1.

For precipitation (Fig. 6), QTCM2 manifests the principal DJF tropical spatial features as seen in the CMAP data in the broadest sense at both resolutions, but there are significant differences, beyond simply the sharpness of the gradients, between the low-resolution and high-resolution models. For tropical land regions, precipitation maxima are present over Africa, the maritime continent, and South America. Structurally, these maxima tend to comprise single centers in the low resolution version (Fig. 6c) but multiple centers at higher resolution (Fig. 6b). ITCZs are evident over the Atlantic, Indian, and eastern Pacific Oceans, although these are generally weak compared to the observations. The East Pacific ITCZ is also located somewhat too far south of its observed DJF position. At least for DJF, the ITCZ structure appears to be better captured than in QTCM1, which is consistent with the arguments presented in SN06, although the improvements may not be as pronounced as in the axisymmetric model. Perhaps unsurprisingly, the simulation of narrow features such as ITCZs is rather sensitive to model resolution. The tilted, tropical-subtropical South Pacific and South Atlantic Convergence Zones (SPCZ and SACZ) are present, but penetrate too far into the (non-deep convecting) dry descent regions over the southeastern tropical Pacific and Atlantic Oceans. In the tropical West Pacific, there is also a large precipitation dipole bias between the SPCZ and the eastern coast of Australia.

4. Isolating how the implementation of QTCM2 impacts precipitation

289 In this section, we are interested in further assessing how the implementation of the new physics
290 in QTCM2 contributes to the model's precipitation behavior. For the results discussed hereafter
291 we consider the coarse resolution simulations unless otherwise noted.
292
293 **4.1 Overview of QTCM1 precipitation behavior**
294 Since we are interested in how inclusion of the ABL modes impacts the simulated precipitation
295 in QTCM2, we briefly highlight a few aspects of the precipitation field as simulated by its
296 predecessor model, QTCM1. (For reference, the QTCM1 DJF precipitation field at the coarse
297 resolution is depicted in Fig. 7.) In general, QTCM2 produces stronger oceanic ITCZs than does
298 QTCM1; furthermore, QTCM2 tends to produce less rainfall over tropical land than does
299 QTCM1. Thus, while QTCM1 greatly underestimates the ratio of oceanic to land region
300 precipitation in the tropics relative to the observations, this ratio is improved (albeit still too low)
301 in QTCM2.
302
303 **4.2 Precipitation sensitivity to added physics in QTCM2**
304 As noted in Section 2, implementation of QTCM2 differs from QTCM1 in three principal ways:
305 (i) *model physics associated with the boundary layer degree of freedom*; (ii) *model*
306 *parameterization schemes*; and (iii) *model parameters*. In this section, we consider how these
307 differences impact the simulation, especially precipitation. To address the model sensitivity to
308 the addition of a decoupled ABL, we consider a model configuration in which temperature and
309 moisture are obtained from vertically-averaged tendencies of ABL and FT temperature and
310 moisture and ABL values of dry static energy and moisture prescribed to FT T_1 and q_1
311 extrapolated to their mean values in the ABL:

$$\frac{dT_1'}{dt} = \frac{\Delta p_f (dT_1/dt) + \Delta p_b (ds_b/dt)}{a_1^f \Delta p_f + a_1^b \Delta p_b}; \quad s_b' = a_1^b T_1$$

$$\frac{dq_1'}{dt} = \frac{\Delta p_f (dq_1/dt) + \Delta p_b (dq_b/dt)}{b_1^f \Delta p_f + b_1^b \Delta p_b}; \quad q_b' = b_1^b q_1 \tag{6}$$

Momentum is slaved by setting ABL zonal and meridional winds to the total (barotropic+baroclinic) velocity at the base of the FT. Additionally, the tendencies of FT barolinic wind momentum are adjusted to account for the affect of ABL convergence on forcing the FT baroclinic mode, while the barotopic mode is constrained to be nondivergent as in QTCM1. Thus:

$$\frac{d\mathbf{v}_1'}{dt} = \frac{\Delta p_f V_1^{2F} (d\mathbf{v}_1/dt) + \Delta p_b V_{1pe} (d/dt)(\mathbf{v}_b - \mathbf{v}_0)}{\Delta p_f V_1^{2F} + \Delta p_b V_{1pe}^2}; \quad \mathbf{v}_b' = \mathbf{v}_0 + V_{1pe}\mathbf{v}_1 \tag{7}$$

Relative to the baseline QTCM2 simulation, DJF precipitation is generally weakened when the ABL and FT are slaved (Fig. 8a; light gray shading depicts where precipitation in the coupled modes configuration is reduced relative to the baseline). In fact, for the tropical regions which are more weakly convecting in the model, precipitation is reduced by 50% or more when the ABL and FT are slaved. Some of these regions which are sensitive to the presence or absence of PBL dynamics are also weakly convecting in observations, while others are more strongly convecting in observations but biased dry in the model, particularly in the absence of PBL dynamics. The East Pacific ITCZ in particular is largely suppressed with ABL-FT slaving, consistent with the arguments of SN06 (see also Sobel 2007). Such behavior broadly mirrors the precipitation differences between the baseline QTCM2 and QTCM1 (Figs. 6c and 7, respectively).

By separately slaving ABL and FT thermodynamic and dynamic modes, we can infer the contributions of each of the added thermodynamic and dynamic degrees of freedom to the

differences in QTCM2. Like the precipitation differences in Fig. 8a, those associated with coupled thermodynamics (Fig. 8c) are largely negative throughout the Tropics, except along certain convective margins such as the northern edge of the western Pacific warm pool/East Pacific ITCZ. The effect of coupling dynamics, by contrast, produces both negative and positive differences relative to the baseline case (Fig. 8b). Indeed, when ABL and FT momentum modes are slaved, DJF precipitation is enhanced over much of the western Pacific warm pool but weakened in the eastern Pacific ITCZ. The presence of nonlinearities such as those in the model deep convection scheme gives rise to some modest regional scale differences between the differences in Fig. 8a and the sum of differences in Figs. 8b and 8c.

One of the principal objectives in constructing a two-level QTCM in SN06 was to achieve better simulation of features such as ITCZs, for which ABL convergence and the Lindzen-Nigam mechanism are expected to play a role. The results here confirm that the added physics in the full QTCM2 have a demonstrable impact.

4.3 Sensitivity to the revised deep convection scheme

We also consider the impact of the convection scheme in QTCM2 by implementing a convection scheme closer to the existing scheme in QTCM. In this implementation, CAPE (or a CAPE-related quantity) is computed over the entire depth of the troposphere using tropospheric-averaged temperature $\langle T \rangle$ and moisture $\langle q \rangle$, namely:

$$\begin{matrix} \langle T \rangle \\ \langle q \rangle \end{matrix} = \begin{cases} \frac{\Delta p_b s_b + \Delta p_f a_1^f T_1}{\Delta p_b + \Delta p_f} + \langle T_{ref} \rangle \\ \frac{\Delta p_b q_b + \Delta p_f b_1^f q_1}{\Delta p_b + \Delta p_f} + \langle q_{ref} \rangle \end{cases} \tag{8}$$

352 The tropospheric-averaged deep convective heating rate, Qc_t, is equivalent to CAPE divided by
353 the timescale for convective adjustment τ_c, i.e.,:

354 $$Qc_t = \frac{CAPE}{\tau_c} = \frac{\langle T_c \rangle - \langle T \rangle}{\tau_c}; \quad CAPE > 0 \tag{9}$$

355 where $\langle T_c \rangle$ is a vertically-averaged convective reference temperature profile. Assuming
356 total enthalpy is conserved during deep convection, the sum of convective heating and
357 convective drying, Qq_t, is zero. ABL convective heating and drying are computed as in the
358 standard configuration of QTCM2, i.e., assuming a boundary layer moist static energy
359 perturbation, while FT convective heating and drying are obtained as residuals based on the total
360 heating and drying and the ABL values.

361 Differencing the QTCM1 convection configuration from the baseline QTCM2 shows
362 increasing precipitation along many of tropical convective margins (Fig. 9). At the same time,
363 within the cores of convecting regions, precipitation rates decrease with the implementation of
364 QTCM1 deep convection. The former likely results from the condition of positive CAPE for the
365 triggering of deep convection, which becomes a weaker constraint with the alternative
366 computation of CAPE, while the latter likely results from compensating mechanisms between
367 margins and cores of the convecting regions. We note that the stronger precipitation in the
368 Pacific and Atlantic ITCZs with the QTCM1 scheme implies that enhancement of the ITCZs due
369 to the additional vertical degree of freedom into QTCM2 has been partially compensated by the
370 change in convective closure described in SN06, and this may be of interest for examination in
371 future work.

372

373

374 **4.4 Sensitivity to revised parameters**

375 Reverting to the vertical structure functions $a_1(p)$, $b_1(p)$, and $V_1(p)$ used in QTCM1 (Fig. 10)
376 causes precipitation within regions of strongest tropical deep convection to intensify and become
377 more localized: within the cores of these regions, precipitation rates of ~30 mm day^{-1} are
378 simulated. On the other hand, precipitation is strongly suppressed everywhere outside of the
379 strongest convecting regions. The results presented here suggest that the revised or altered
380 model parameters and parameterizations play a significant, nontrivial role in accounting for
381 differences between QTCM2 and QTCM1. In fact, such the differences attributable to parameter
382 or parameterization changes are comparable to, or may even locally exceed, those associated
383 with the additional physics.

384

385 **5. Sensitivity analyses for deep and shallow convection and FT moisture**

386 As a demonstration of the utility of the QTCM2 framework, we consider here some aspects of
387 model convection schemes that are poorly constrained. Because simulated convective processes
388 in climate models are very sensitive to parameterization (Jackson et al. 2008), it is clearly of
389 interest to explore how tropospheric moisture and precipitation are related in convective
390 parameterizations.

391

392 **5.1 Sensitivity to deep convective adjustment timescale**

393 One of the parameters poorly constrained in QTCM2 and many other models with similar
394 convection schemes is the convective adjustment timescale τ_c, i.e., the time necessary to
395 consume CAPE and relax the convective instability (Jackson et al. 2008). While the deep
396 convective adjustment timescale was set to 2 hours in Betts and Miller (1986), Bretherton et al.

(2004) have shown this parameter to be strongly scale dependent, with values that may be up to an order of magnitude larger. Note that the precipitation rate in QTCM2 is equivalent to the total deep convective heating rate averaged over the depth of the troposphere, since there is no stratiform precipitation.

A comparison of QTCM2-simulated precipitation for January for τ_c of 6 hours, the default value assumed in QTCM2, and 2 hours, as assumed in QTCM1, is presented in Fig. 11a. The most prominent difference here is the disappearance of the East Pacific ITCZ as τ_c is decreased. To see this, we note that the differences along the east Pacific ITCZ as depicted in Fig. 11a are comparable to the baseline precipitation rates in Fig. 6c. On the other hand, peak precipitation rates in the core regions of tropical deep convection, such as near the maritime continent, are typically enhanced as τ_c becomes smaller.

To provide further insight into the precipitation sensitivity to the rate of deep convective adjustment, Fig. 11b illustrates ABL and FT moisture differences for the two cases (2 hours minus 6 hours). Within the most strongly convecting tropical regions, ABL moisture (shading; in g kg^{-1}) is typically reduced for small τ_c. On the other hand, moister ABL conditions tend to prevail along the margins of strong tropical deep convection for τ_c = 2 hours. Within the FT, moisture loading is generally lower throughout the entire tropical troposphere for lower τ_c, as is total column water vapor.

Our interpretation of these results is as follows. In strongly convecting regions or at times when strong tropical deep convection is present, lowering τ_c renders the local FT moisture sink more efficient, so that when the conditions for deep convection are met, moisture is rapidly removed. The faster removal of FT moisture within strongly convecting regions means that, away from these regions, less moisture will generally be available, as FT moisture transport into

adjacent regions will be reduced. In marginally-convecting regions, the FT drying is especially crucial—even as the ABL itself is more humid at lower τ_c, the triggering of deep convection is inhibited by the drier FT. With faster deep convective adjustment, FT convective heating in strongly convecting cores is also enhanced; the additional heating in regions of deep convection sets up anomalous Gill-like responses that warm and dry the entire tropical FT.

5.2 Sensitivity to shallow convective adjustment timescale

Here we consider sensitivity of QTCM2 to τ_{sh} by comparing the baseline simulation to one for which the shallow convective times are increased by a factor of 10 ("slow shallow adjustment"). Fig. 12a illustrates the January precipitation differences between the slow shallow and baseline simulations. It can be seen that damping shallow convective adjustment is associated with decreasing marginal precipitation rates and (slightly) increasing precipitation away from the margins, although not necessarily where deep convection and precipitation tend to be strongest in the baseline simulation. With slow shallow convective adjustment, the ABL is strongly moistened just to the north of the equator outside of the strong convecting region (Fig. 12b), with widespread reduction in free tropospheric moistening throughout the Tropics.

The shallow convective sensitivity results described here are consistent with Neggers et al. (2007; e.g., c.f. Fig. 4c of Neggers et al. (2007), which is for July rather than January). Of course, the version of QTCM used by Neggers et al. (2007) had two modes in moisture but retained the single mode in temperature and associated momentum modes from QTCM1. We note that altering shallow convective adjustment in each of moisture and temperature separately is found to have additive effects, with roughly half of total response coming from the moisture and temperature adjustments.

443

444 **5.3 Decreasing subsaturation**

445 A planned target for future work is to implement a mass flux scheme into QTCM2 by suitable
446 projection of such a scheme onto QTCM2 basis functions. Of course, inclusion of a mass flux
447 scheme in QTCM2 will require taking into account the effects of various processes, including
448 entrainment, detrainment, subsidence, rain reevaporation, and at present, it is not obvious how
449 this should be done. However, in anticipation of such an approach, we consider two simplifying
450 approaches that might be viewed as approximating some features of an entraining plume model.
451 The first approach is to adjust the subsaturation parameter, α, appearing in the computation of
452 the FT convective reference profile. The Betts-Miller scheme uses this subsaturation parameter
453 in its moisture reference profile (toward which moisture is adjusted) to loosely mimic the bulk
454 impact of condensation, conversion to precipitating hydrometeors, precipitation, detrainment and
455 reevaporation processes that would occur in a plume model without the need for detailed
456 consideration of all processes involved.

457 Fig. 13 depicts the impact of uniformly reducing the default vertical subsaturation profile by
458 20%. Overall, lowering α tends to enhance precipitation along tropical convective margins or
459 narrow ITCZs (e.g., the East Pacific ITCZ) while reducing precipitation within the core regions
460 (Fig. 13a). Moreover, the decrease in the subsaturation profile is associated with weak increases
461 to ABL moisture where marginal precipitation is enhanced but decreases in ABL moisture
462 elsewhere and with pervasive drying of the FT. To understand these changes, we note that
463 lowering α reduces the target for the convective adjustment, so that the troposphere ultimately
464 adjusts toward a drier state. At the same time, the convective threshold condition, $q > q_c(T)$, is
465 lowered, so convection can occur at lower ambient moisture; thus, precipitation in marginal

466 regions can increase and/or expand. One subtlety here is that the lowering of $q_c(T)$ associated
467 with lower subsaturation is somewhat offset by increased warming in the free troposphere, which
468 drives up the saturation values and thus reduces convective instability. The overall pattern for
469 lower subsaturation resembles the (inverse of) the rich-get-richer mechanism (Neelin et al.
470 2003).
471
472 **5.4 Adding an entrainment-like process**
473 The second approach for approximating a more realistic entraining type model in QTCM2
474 involves adding an entrainment-like process to the convective closure, specifically one that
475 mimics the effect of free tropospheric moisture on plume temperature structure. Indeed, the
476 baseline convection scheme in QTCM2, like in QTCM1, assumes a parcel associated with a
477 given ABL moist static energy perturbation would follow a moist adiabat through the FT, so that
478 no effect of environmental mixing is assumed. To include one of the most important effects of
479 entrainment, we modify the computation of the convective reference temperature in the deep
480 convection scheme by including a term proportional to the FT moisture deficit relative to
481 saturation. This simple form is suggested by recent results of Sahany et al. (2012) showing how
482 entraining CAPE decreases as a function of FT relative humidity and the strength of entrainment.
483 Enabling the simple entrainment-like term leads to decreased precipitation along tropical
484 convective margins (Fig. 14a), which is consistent with expectations, since regions bounding the
485 convection zones are likely to be farther from saturation, such that entrainment of relatively dry
486 air there leads to an increase in the plume lapse rate in the free troposphere, which will tend to
487 reduce the CAPE-like quantity $(T - T_c)$, with attendant reduction in convective precipitation. .
488 Core convecting regions are seen to experience increasing precipitation when the entrainment-

like term is enabled. Such behavior likely represents the operation of processes involving elements of the rich-get-richer mechanism and the feedbacks discussed by Neggers et al. (2007). The moisture required for convective instability is slightly increased for a given large-scale temperature due to the entrainment-like effect. Reduction in rainfall near the convective margins would yield a slight reduction in tropospheric temperature if this were not compensated by other adjustments. Constraints applying to a tropics-wide scale lead to slight adjustments in tropospheric temperature to keep to convective heating averaged over the entire Tropics from changing as strongly as occurs locally. This leaves the core of the convective regions at a slight advantage for convective instability relative to the convective margins. The moisture that fails to precipitate out in marginal regions ultimately winds up within the convecting core regions. Similar effects in the response to entrainment can be seen in full climate models (Oueslati and Bellon 2012b).

6. Summary and conclusions

In this paper, we describe the implementation of the Quasi-equilibrium Tropical Circulation Model 2 (QTCM2), a two-level intermediate level complexity model. Following the approach of Sobel and Neelin (2006), a prognostic atmospheric boundary layer of fixed depth is added. Free-tropospheric basis functions are re-defined accordingly between the boundary layer top and nominal tropopause, but are otherwise similar to those used in QTCM1. Projecting the primitive equations on the BL plus FT yields twice as many prognostic equations as in QTCM1 for thermodynamic quantities, and one new set of momentum equations for the PBL in addition to the baroclinic and barotropic free-tropospheric modes.

511 QTCM2 is shown to produce reasonable climatologies of temperature, moisture, winds, and
512 precipitation. While some aspects of the simulated behavior in QTCM2 do improve relative to
513 the predecessor model (QTCM1)—e.g., partitioning of land versus ocean precipitation—not all
514 features are clearly improved. Despite this, we maintain that the model's utility lies in
515 applications to problems for which the original model was not suited, such as addressing the
516 influence of FT moisture on tropical deep convection.

517 As noted in SN06 and several studies with idealized versions of QTCM2 (Bellon and Sobel
518 2008a, 2008b, 2010), the addition of ABL physics does produce some differences relative to the
519 single mode predecessor, such as the strengthening of precipitation in Intertropical Convergence
520 Zones (ITCZs). It should be pointed out, however, that changes to model parameters, stemming
521 primarily from use of revised vertical structure functions, as well as model parameterizations are
522 found to impact QTCM2-simulated precipitation as much as the added physics. In light of
523 QTCM2's sensitivity to parameter changes, we suggest that the model may represent a useful
524 testbed for parameter optimization techniques.

525 We also document some aspects of QTCM2's convective sensitivity to FT moisture.
526 Adjustments to the model convection scheme, such as alterations to the tropospheric
527 subsaturation profile or inclusion of FT entrainment, demonstrate how basic physical processes
528 impact QTCM2-simulated precipitation. From various convective sensitivity experiments
529 conducted, we note several common features in the simulated precipitation response, namely: (i)
530 increasing precipitation is associated with increasing column water vapor; (ii) strengthening of
531 vertical moisture gradients, with either larger increases or smaller decreases in ABL moisture
532 relative to the FT, is associated with decreasing precipitation; and (3) feedbacks between moist
533 dynamics and convective processes may produce complex spatial behavior. The occurrence of

trade-offs between precipitation sensitivity in the core convecting regions and their margins, and the mechanisms for these trade-offs, may provide prototypes for interpreting similar sensitivity evident in more complex models.

Finally, we note several targets for future model improvement, including implementation of a cumulus mass flux scheme; revised cloud prediction, especially the addition of an explicit stratocumulus parameterization; and the addition of large-scale precipitation. In the spirit of community-oriented model development, we welcome and encourage efforts to refine or add to QTCM2 physics and parameterizations.

Acknowledgments

We thank Chia Chou, Matt Munnich, Pierre Gentine, and Roel Neggers for discussion, Chris Holloway for providing the revised vertical structure functions, and Joyce Meyerson for graphical assistance. Financial support was provided by National Science Foundation grant AGS-1103209.

Appendix A

The horizontal velocity, $\mathbf{v} = (u, v)$; pressure vertical velocity ω; temperature T in energy units, i.e., temperature in Kelvin multiplied by c_p, the heat capacity of air at constant pressure; and specific humidity q in energy units, i.e., specific humidity in kg kg^{-1} multiplied by the latent heat of vaporization L_v, satisfy the primitive equations in pressure coordinates:

$$\frac{d\mathbf{v}}{dt} + \omega\partial_p\mathbf{v} + f\hat{\mathbf{k}} \times \mathbf{v} = -\nabla\varphi + \mathbf{F}_v \tag{A1}$$

$$\frac{dT}{dt} + \omega\partial_p s = Q_c + Q_R \tag{A2}$$

$$\frac{dq}{dt} + \omega \partial_p q = Q_q \tag{A3}$$

$$\partial_p \omega + \nabla \cdot \mathbf{v} = 0 \tag{A4}$$

where f is the Coriolis parameter, φ the geopotential, $\mathbf{F}_v$ the frictional force, Q_R the radiative heating, and Q_c and Q_q are the convective heat source and moisture sink respectively. Here, $\frac{d}{dt} = \partial_t + \mathbf{v} \cdot \nabla$ is the total derivative following horizontal motion and $\nabla \cdot \mathbf{v}$ is the horizontal divergence.

Within the FT, momentum, temperature, and moisture equations can be expressed, as in QTCM1, as:

$$\mathbf{v}(x,y,p,t) = V_0 \mathbf{v}_0(x,y,t) + V_1(p)\mathbf{v}_1(x,y,t) \tag{A5}$$

$$T(x,y,p,t) = T_r(p) + a_1(p)T_1(x,y,t) \tag{A6}$$

$$q(x,y,p,t) = q_r(p) + b_1(p)q_1(x,y,t) \tag{A7}$$

Here, the "barotropic" mode structure function V_0 is independent of pressure in the FT; it is zero-valued in the ABL and is thus not strictly barotropic though the terminology is retained. $V_1(p)$, the profile for the baroclinic mode, is constructed to be consistent with a_1 by hydrostatic balance and is defined with zero mean when integrated over the FT:

$$V_1(p) = a_1^+ - < a_1^+ >^F \tag{A8}$$

where $a_1^+ = \int_{p_t}^{p} a_1(p')d\ln p'$ and the notation $< ... >^F$ denotes the vertical average over the FT. Note that the zero mean of $V_1(p)$ over the depth of the FT renders the baroclinic and barotropic modes orthogonal in the FT.

575 For the implementation of QTCM2, the "bottom" of QTCM1 is lifted and the mixed layer
576 ABL is imposed beneath it. ABL vertical structures for momentum, moisture, and dry static
577 energy are taken as vertically constant within the ABL:

578 $$\mathbf{v}(x,y,p,t) = \mathbf{v}_b(x,y,t) \tag{A9}$$

579 $$s_b(x,y,p,t) = s_{rb} + s_b(x,y,t) \tag{A10}$$

580 $$q_b(x,y,p,t) = q_{rb} + q_b(x,y,t) \tag{A11}$$

581 For pressure velocity, the vertical structure function $\Omega_1(p)$ is obtained from the continuity
582 equation (A4):

583 $$\Omega_1(p) = \int_{p_t}^{p_e} V_1(p')dp', \quad p_t < p < p_e, \quad 0 \text{ otherwise} \tag{A12}$$

584 The orthogonality of the FT barotropic and baroclinic modes requires $\Omega_1(p_e) = 0$ and further
585 necessitates ABL mass convergence (divergence) be balanced by FT barotropic mass divergence
586 (convergence), i.e.,

587 $$\Delta p_b \nabla \cdot \mathbf{v}_b = -\Delta p_f \nabla \cdot \mathbf{v}_0 = \omega(p_e) \tag{A13}$$

588 Thus, the total vertical velocity field is

589 $$\omega(x,y,p,t) = -\Omega_0 \nabla \cdot \mathbf{v}_0 - \Omega_1 \nabla \cdot \mathbf{v}_1 \tag{A14}$$

590 where $\Omega_0 = \begin{cases} p - p_t & p_t < p < p_e \\ (p_s - p)\Delta p_f / \Delta p_b & p_e < p < p_s \end{cases}$. With the definitions outlined above, the
591 primitive equations can be projected and the vertically-averaged parameters in Table 1 obtained.
592

References Cited

Back, L. E., and C. S. Bretherton, 2009: On the relationship between SST gradients, boundary layer winds and convergence over the tropical oceans. *J. Clim., 22,* 4182-4196.

Bellon, G., and A. H. Sobel, 2008a: Poleward-propagating intraseasonal monsoon disturbances in an intermediate-complexity axisymmetric model. *J. Atmos. Sci., 65*, 470—489.

Bellon, G., and A. H. Sobel, 2008b: Instability of the axisymmetric monsoon flow and intraseasonal oscillation. *J. Geophys. Res.-Atmos.*, *113*, D07108.

Bellon G., A. H. Sobel, and J. Vialard, 2008: Ocean-atmosphere coupling in the monsoon intraseasonal oscillation: a simple model study. *J. Clim*., *21*, 5254–5270.

Bellon G. and A. H. Sobel, 2010: Multiple equilibria of the Hadley circulation in an intermediate-complexity model. *J. Clim*., *23*, 1760–1778.

Bellon G., 2011: Monsoon intraseasonal oscillation and land-atmosphere interaction in an idealized model, *Clim. Dyn.*, *37*, 1081–1096.

Biasutti, M., A. H. Sobel, and Y. Kushnir, 2006: GCM precipitation biases in the tropical Atlantic. *J. Clim., 19*, 935–958.

Burns, S.P., A. H. Sobel, and L.M. Polvani, 2006: Asymptotic solutions to the moist axisymmetric Hadley circulation. *Theor. Comp. Fluid Dyn*., *20*, 443—467.

Bretherton, C.S., and A. H. Sobel, 2002: A simple model of a convectively coupled Walker circulation using the weak temperature gradient approximation. *J. Clim., 15*, 2907–2920.

Bretherton, C. S., M. E. Peters, and L. Back, 2004: Relationships between water vapor path and precipitation over tropical oceans. *J. Clim., 17*, 1517–1528.

Chiang, J.C.H., and A. H. Sobel, 2002: Tropical tropospheric temperature variations caused by ENSO and their influence on the remote tropical climate. *J. Clim., 15*, 2616–2631.

Chou, C., and J. D. Neelin, 1996: Linearization of a longwave radiation scheme for intermediate tropical atmospheric models. *J. Geophys. Res., 101*, 15,129—15,145.

Chou, C., and J. D. Neelin, 2003: Mechanisms limiting the northward extent of the northern summer convection zones. *J. Clim., 16*, 406-425.

Chou, C., and J. D. Neelin, 2004: Mechanisms of global warming impacts on regional tropical precipitation. *J. Clim., 17*, 2688–2701.

Cuijpers, H., and Bechtold, P., 1995: A simple parameterization of cloud water related variables

for use in boundary layer models. *J. Atmos. Sci., 52*, 2486–2490

Dai, A., 2006: Precipitation characteristics in eighteen coupled climate models. *J. Clim., 19*, 4605–4630.

Del Genio, A.D., 2011: Representing the sensitivity of convective cloud systems to tropospheric humidity in general circulation models. *Surv. Geophys.*, doi:10.1007/s10712-011-9148-9.

Derbyshire, S. H., I. Beau, P. Bechtold, J.-Y. Grandpeix, J.-M. Piriou, J.-L. Redelsperger, and P. M. M. Soares, 2004: Sensitivity of moist convection to environmental humidity. *Quart. J. Roy. Meteor. Soc., 130*, 3055–3080.

Frierson, D. M., 2007: Convectively Coupled Kelvin Waves in an Idealized Moist General Circulation Model. *J. Atmos. Sci., 64*, 2076—2090.

Grabowski, W. W., and M. W. Moncrieff, 2004: Moisture-convection feedback in the tropics. *Q. J. R. Meteor. Soc., 130*, 3081—3104.

Grabowski, W. W., 2006: Impact of Explicit Atmosphere–Ocean Coupling on MJO-Like Coherent Structures in Idealized Aquaplanet Simulations. *J. Atmos. Sci., 63*, 2289–2306.

Hannah, W. M., and E. D. Maloney, 2011: The Role of Moisture–Convection Feedbacks in Simulating the Madden–Julian Oscillation. *J. Clim., 24*, 2754–2770. doi: 10.1175/2011JCLI3803.1

Holloway, C. E., and J. D. Neelin, 2007: The convective cold top and quasi equilibrium. *J. Atmos. Sci., 64*, 1467–1487.

Holloway, C. E., and J. D. Neelin, 2009: Moisture vertical structure, column water vapor, and tropical deep convection. *J. Atmos. Sci., 66*, 1665–1683.

Holloway, C. E., and J. D. Neelin, 2010: Temporal relations of column water vapor and tropical precipitation. *J. Atmos. Sci., 67*, 1091—1104.

Jackson, C. S., M. K. Sen, G. Huerta, Y. Deng, and K. P. Bowman, 2008: Error reduction and convergence in climate prediction. *J. Clim., 21*, 6698–6709 doi: 10.1175/2008JCLI2112.1.

Kanamitsu, M., W. Ebisuzaki, J. Woollen, S-K Yang, J.J. Hnilo, M. Fiorino, and G. L. Potter, 2002: NCEP-DEO AMIP-II Reanalysis (R-2). *Bull. Amer. Meteor. Soc., 83*, 1631—1643.

Khouider, B., and A. J. Majda, 2006: A Simple Multicloud Parameterization for Convectively Coupled Tropical Waves. Part I: Linear Analysis. *J. Atmos. Sci., 63*, 1308—1323.

Kim, D., A. H. Sobel, E. D. Maloney, D. M. W. Frierson, and I.-S. Kang, 2011: A Systematic Relationship between Intraseasonal Variability and Mean State Bias in AGCM Simulations. *J. Clim., 24*, 5506-5520

Kuang, Z., and C. S. Bretherton, 2007: A mass flux scheme view of a high-resolution simulation of a transition from shallow to deep cumulus convection. *J. Atmos. Sci., 63*, 1895—1909.

Lin, J.W., J. D. Neelin, and N. Zeng, 2000: Maintenance of tropical intraseasonal variability: impact of evaporation-wind feedback and midlatitude storms. *J. Atmos. Sci., 57*, 2793–2823.

Lindzen, R. S., and S. Nigam, 1987: On the role of sea surface temperature gradients in forcing low-level winds and convergence in the tropics. *J. Atmos. Sci., 44*, 2418—2436.

Lintner, B.R. and J.C.H. Chiang, 2007: Adjustment of the remote tropical climate to El Niño conditions. *J. Clim., 20*, 2544—2557, doi:10.1175/JCLI4138.1.

Lintner, B. R. and J. D. Neelin, 2007: A prototype for convective margin shifts. *Geophys. Res. Lett., 34*, L05812, doi:10.1029/2006GL027305.

Lintner, B. R. and J. D. Neelin, 2008: Eastern margin variability of the South Pacific Convergence Zone. *Geophys. Res. Lett., 35*, L16701, doi:10.1029/2008GL034298.

Lintner, B.R., P. Gentine, K.L. Findell, F. D'Andrea, and A.H. Sobel, 2012: An idealized prototype for large-scale land-atmosphere coupling. *Revised for J. Clim*.

Neggers, R., B. Stevens and J. D. Neelin, 2006: A simple equilibrium model for shallow cumulus convection. *Theor. Comp. Fluid Dyn*., *20*, 305-322.

Neggers, R. A. J., J. D. Neelin, and B. Stevens, 2007: Impact mechanisms of shallow cumulus convection on tropical climate dynamics. *J. Clim., 20*, 2623—2642.

Neelin, J. D., and N. Zeng, 2000: A quasi-equilibrium tropical circulation model—formulation. *J. Atmos. Sci.*, *57*, 1741–1766.

Neelin, J. D., C. Chou, and H. Su, 2003: Tropical drought regions in global warming and El Niño teleconnections. *Geophys. Res. Lett., 30*, 2275. doi:10.1029/2003GL018625.

Neelin, J. D., and H. Su, 2005: Moist teleconnection mechanisms for the tropical South American and Atlantic sector. *J. Clim.*, *18*, 3928–3950.

Oueslati, B., and G. Bellon, 2012a: Tropical precipitation regimes and mechanisms of regime transitions : contrasting two aquaplanet general circulation models. *Clim. Dyn*., in press.

Oueslati, B., and G. Bellon, 2012b: Convective entrainment and large-scale organization of tropical precipitation: sensitivity of the CNRM-CM5 hierarchy of models. *Submitted to J. Clim.*

Parsons, D. B., K. Yoneyama, and J.-L. Reddelsperger, 2000: The evolution of the tropical western Pacific atmosphere-ocean system following the arrival of a dry intrusion. *Quart. J. Roy. Meteor. Soc., 126,* 517–548.

Sahany, S., J. D. Neelin, K. Hales, and R. Neale, 2012: Temperature-moisture dependence of the deep convective transition as a constraint on entrainment in climate models. *J. Atmos. Sci., in Press.*

Sherwood, S. C., P. Minnis, and M. McGill, 2004: Deep convective cloud top heights and their thermodynamic control during CRYSTAL-FACE. *J. Geophys. Res., 109*, D20119.

Sobel, A.H., and C. S. Bretherton, 2000: Modeling tropical precipitation in a single column. *J. Clim.*, 13, 4378–4392.

Sobel, A. H., J. Nilsson, and L. M. Polvani, 2001: The weak temperature gradient approximation and balanced tropical moisture waves. *J. Atmos. Sci., 58*, 3650—3665.

Sobel, A.H., C.S. Bretherton, H. Gildor, and M.E. Peters, 2004: Convection, cloud-radiative feedbacks and thermodynamic ocean coupling in simple models of the Walker circulation. In: Wang, C., Xie, S.-P., Carton, J.A. (eds.) *Earth's Climate: The Ocean-Atmosphere Interaction.* American Geophysical Union Geophysical Monograph 147, 393–405.

Sobel, A. H., and J. D. Neelin, 2006: The boundary layer contribution to intertropical convergence zones in the quasi-equilibrium tropical circulation model framework. *Theor. Comp. Fluid Dyn*., *20*, 323—350.

Sobel, A. H., 2007: Simple models of ensemble-averaged precipitation and surface wind, given the SST. In *The Global Circulation of the Atmosphere*, T. Schneider and A. H. Sobel, Eds., Princeton University Press.

Su, H., and J.D. Neelin, 2005: Dynamical mechanisms for African monsoon changes during the mid-Holocene. *J. Geophys. Res.-Atmos., 110*, D19105, doi:10.1029/2005JD005806.

Tompkins, A. M., 2001: Organization of tropical convection in low vertical wind shears: The role of water vapor. *J. Atmos. Sci., 58,* 529–545.

Xie P., and P. A. Arkin, 1997: Global precipitation: a 17-year monthly analysis based on gauge observations, satellite estimates, and numerical model outputs. *Bull. Amer. Meteor. Soc.,78*, 2539—2558.

Zeng, N., J. D. Neelin, and C. Chou, 2000: A quasi-equilibrium tropical circulation model–Implementation and simulation. *J. Atmos. Sci.*,, *57*, 1767–1796.

Table Captions

Table 1: Baseline QTCM2 parameter values.

Figure Captions

Fig. 1: Vertical structure functions a1(p), b1(p), and V1(p) used in QTCM2.

Fig. 2: Comparison of DJF 2m temperatures from (a) the NCEP Reanalysis 2 and QTCM2 at (b) high resolution and (c) low resolution. Units are in °C.

Fig. 3: Comparison of DJF 2m specific humidity from (a) the NCEP Reanalysis 2 and QTCM2 at (b) high resolution and (c) low resolution. Units are in g kg^{-1}.

Fig. 4: Comparison of DJF cwv from (a) the NCEP Reanalysis 2 and QTCM2 at (b) high resolution and (c) low resolution. Units are in mm.

Fig. 5: Comparison of DJF winds from (a) the NCEP Reanalysis 2 and QTCM2 at (b) high resolution and (c) low resolution. Shown are boundary layer winds (vectors; values relative to the reference arrow) and 200 mb zonal wind (shading; units of m s^{-1}).

Fig. 6: Comparison of DJF precipitation from (a) CMAP and QTCM2 at (b) high resolution and (c) low resolution. Units are in mm day^{-1}.

Fig. 7: As in Fig. 6, but for QTCM1.

Fig. 8: QTCM2 sensitivity to independent ABL and FT thermodynamics and dynamics. (a) Impact of slaving ABL and FT dynamics and thermodynamics on January precipitation. Gray contours show precipitation differences of the coupled minus baseline simulations, with a contour interval of 1 mm day^{-1} and the zero contour omitted. (Light (dark) gray shading further gridpoints for which the precipitation differences are negative (positive) with a magnitude of at least 0.25 mm day^{-1}.) For reference, January precipitation from the baseline QTCM2 is shown (blue contours). (b) As in (a), but slaving dynamics only. (c) As in (a), but slaving thermodynamics only.

Fig. 9: As in Fig. 8, but for a configuration using QTCM1 vertical structure functions minus the baseline.

Fig. 10: As in Fig. 8, but for a configuration using the QTCM1 deep convection scheme minus the baseline.

Fig. 11: (a) As in Fig. 8, but for a configuration with a deep convective adjustment timescale of 2 hours minus the baseline. (b) ABL and FT moisture differences (shading and contours, respectively), in units of g kg^{-1}.

Fig. 12: As in Fig. 11, but for a configuration with shallow convective adjustment times multiplied by 10 minus the baseline.

Fig. 13: As in Fig. 11, but for a configuration with FT subsaturation decreased by 20% minus the baseline.

Fig. 14: As in Fig. 11, but for a configuration with entrainment added minus the baseline.

824 ***Table 1: Baseline QTCM2 parameter values***

825

Parameter	Value	Definition
p_s, p_e, p_t	1000,900,150 mb	Pressures at the surface, ABL top, and model top (tropopause)
$\langle a_1 \rangle^F, a_{1e}$	0.3958,0.2531	Vertical integral and ABL top value of temperature basis function
$\langle b_1 \rangle^F, b_{1e}$	0.1789,0.5634	Vertical integral and ABL top value of moisture basis function
$\langle a_1^+ \rangle^F$	0.2378	
$\langle a_b^+ \rangle^F$, a_b^{+e}	0.0513,0.1038	
$\langle V_1^2 \rangle^F$, $\langle V_1^3 \rangle^F / \langle V_1^2 \rangle^F$	0.0457,0.2024	
V_{1e}	-0.2378	
$\langle a_1 V_1 \rangle^F$	0.0197	
$T_{rb}, T_{re}, \langle T_r \rangle^F$	302,296.6,263.57 K	Reference ABL, ABL top, and FT temperatures
$q_{rb}, q_{re}, \langle q_r \rangle^F$	51.26,38.84,12.33 K	Reference ABL, ABL top, and FT moistures
M_{sr1}, M_{sr0}	3.27,16.60 K	Reference dry static stabilities
M_{sp1}, M_{sp0}	0,0.2107	Dry static stability changes per T1 change
M_{qr1}, M_{qr0}	1.99,26.50 K	Reference moisture stratifications
M_{qp1}, M_{qp0}	0.0289,0.3844	Moisture stratification changes per q1 change

826

827

Fig. 1

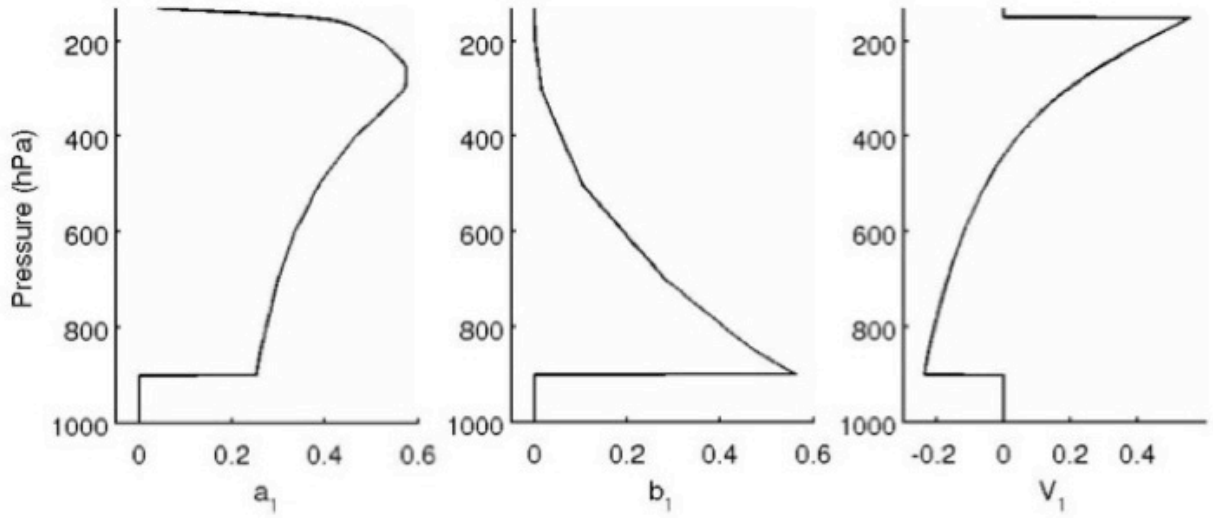

828
829

Fig. 2

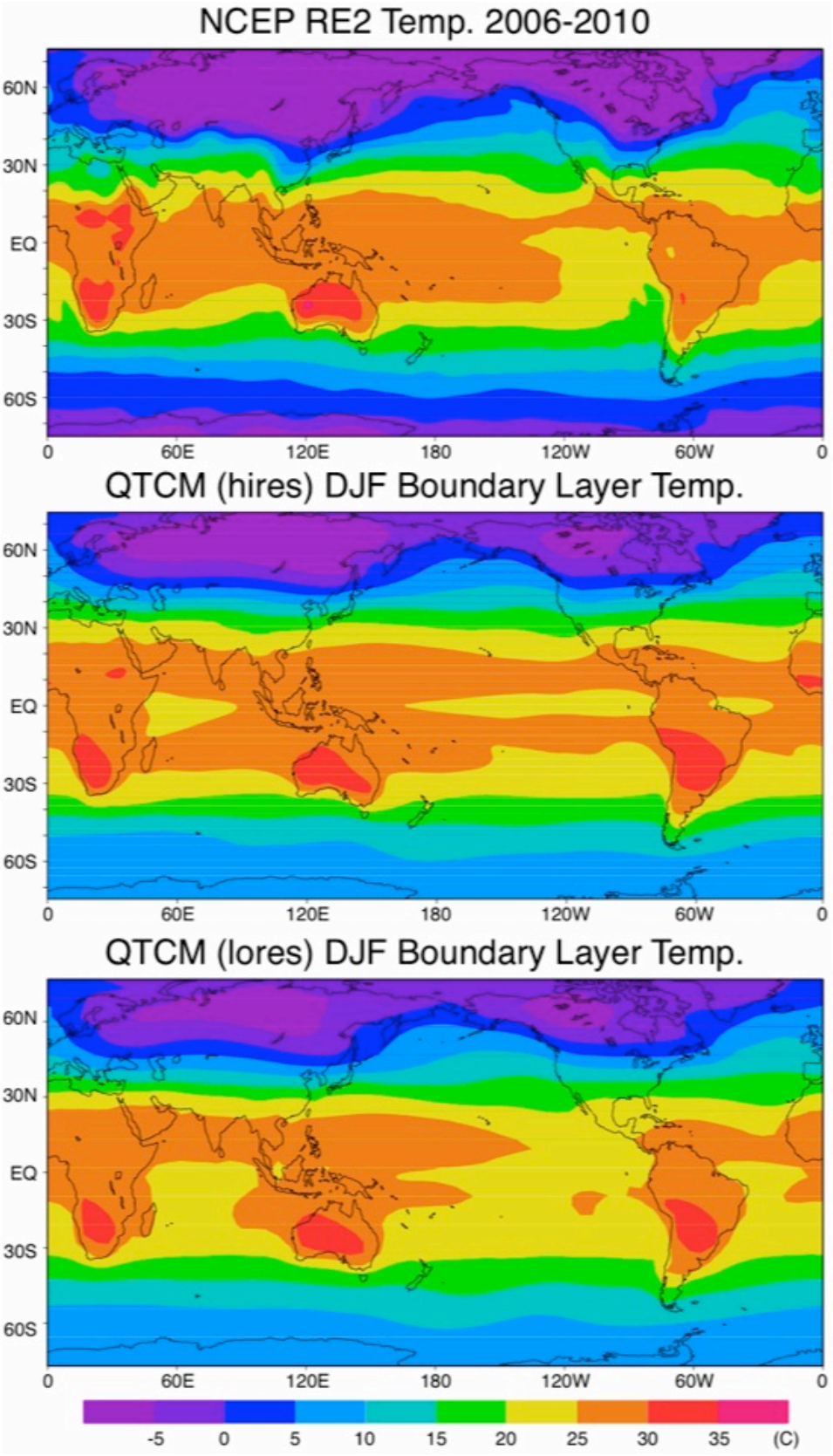
NCEP RE2 Temp. 2006-2010
QTCM (hires) DJF Boundary Layer Temp.
QTCM (lores) DJF Boundary Layer Temp.
60N
30N
EQ
30S
60S
0
60E
120E
180
120W
60W
-5
0
5
10
15
20
25
30
35
(C)

Fig. 3

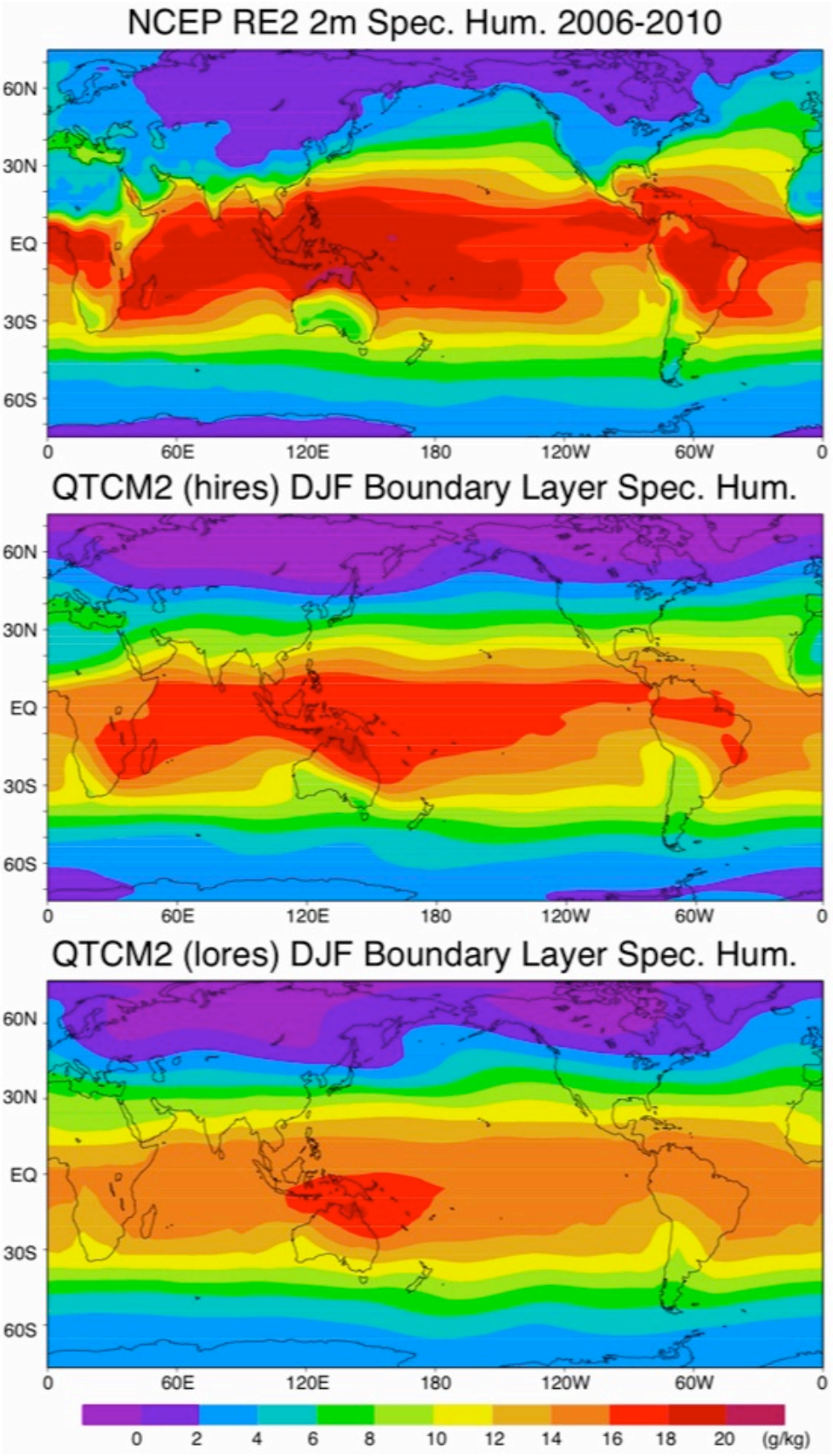
NCEP RE2 2m Spec. Hum. 2006-2010
QTCM2 (hires) DJF Boundary Layer Spec. Hum.
QTCM2 (lores) DJF Boundary Layer Spec. Hum.
60N
30N
EQ
30S
60S
0
60E
120E
180
120W
60W
0 2 4 6 8 10 12 14 16 18 20 (g/kg)

832
833

Fig. 4

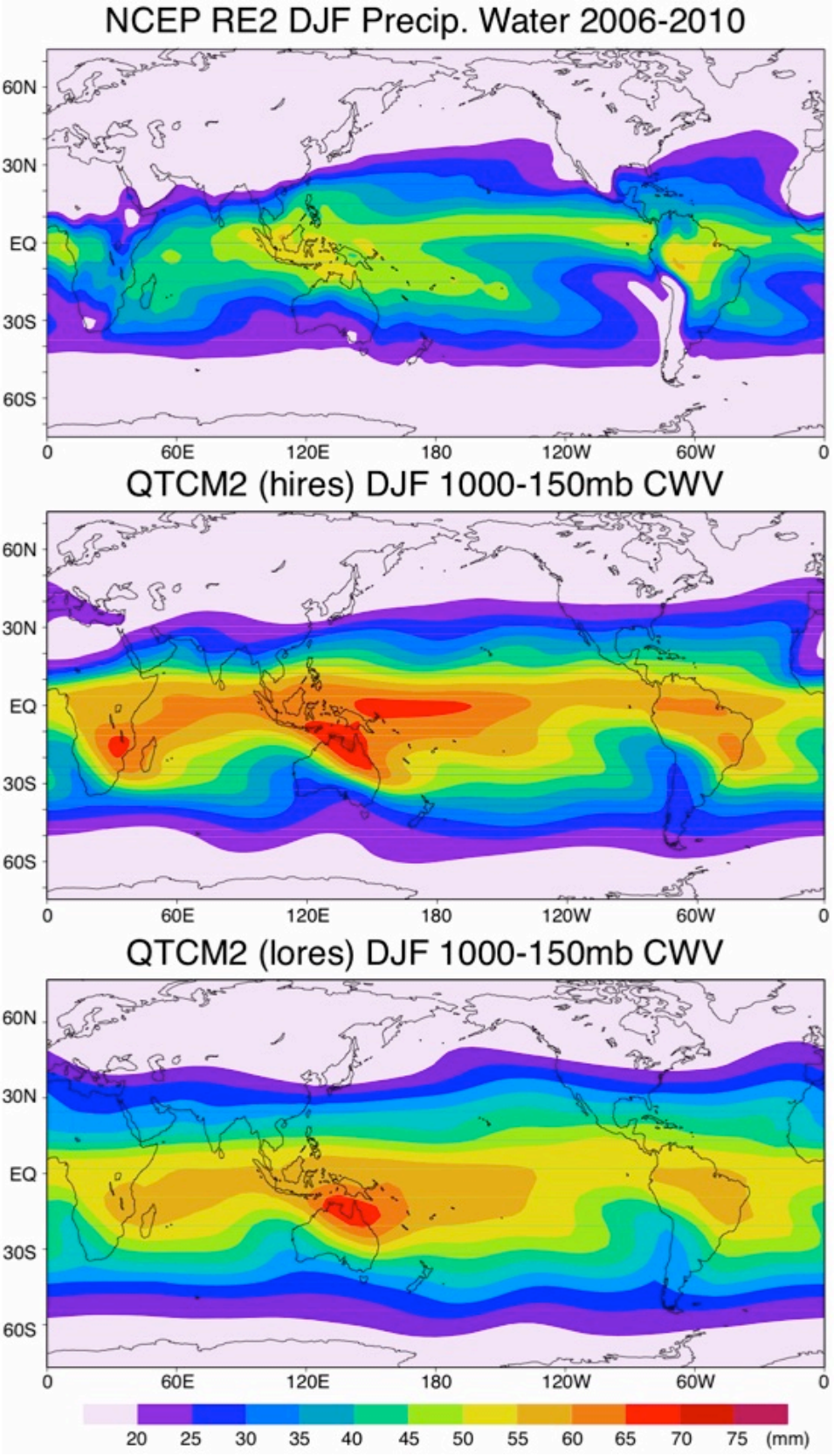
NCEP RE2 DJF Precip. Water 2006-2010
60N
30N
EQ
30S
60S
0
60E
120E
180
120W
60W
0
QTCM2 (hires) DJF 1000-150mb CWV
QTCM2 (lores) DJF 1000-150mb CWV
20 25 30 35 40 45 50 55 60 65 70 75 (mm)

834
835

Fig. 5

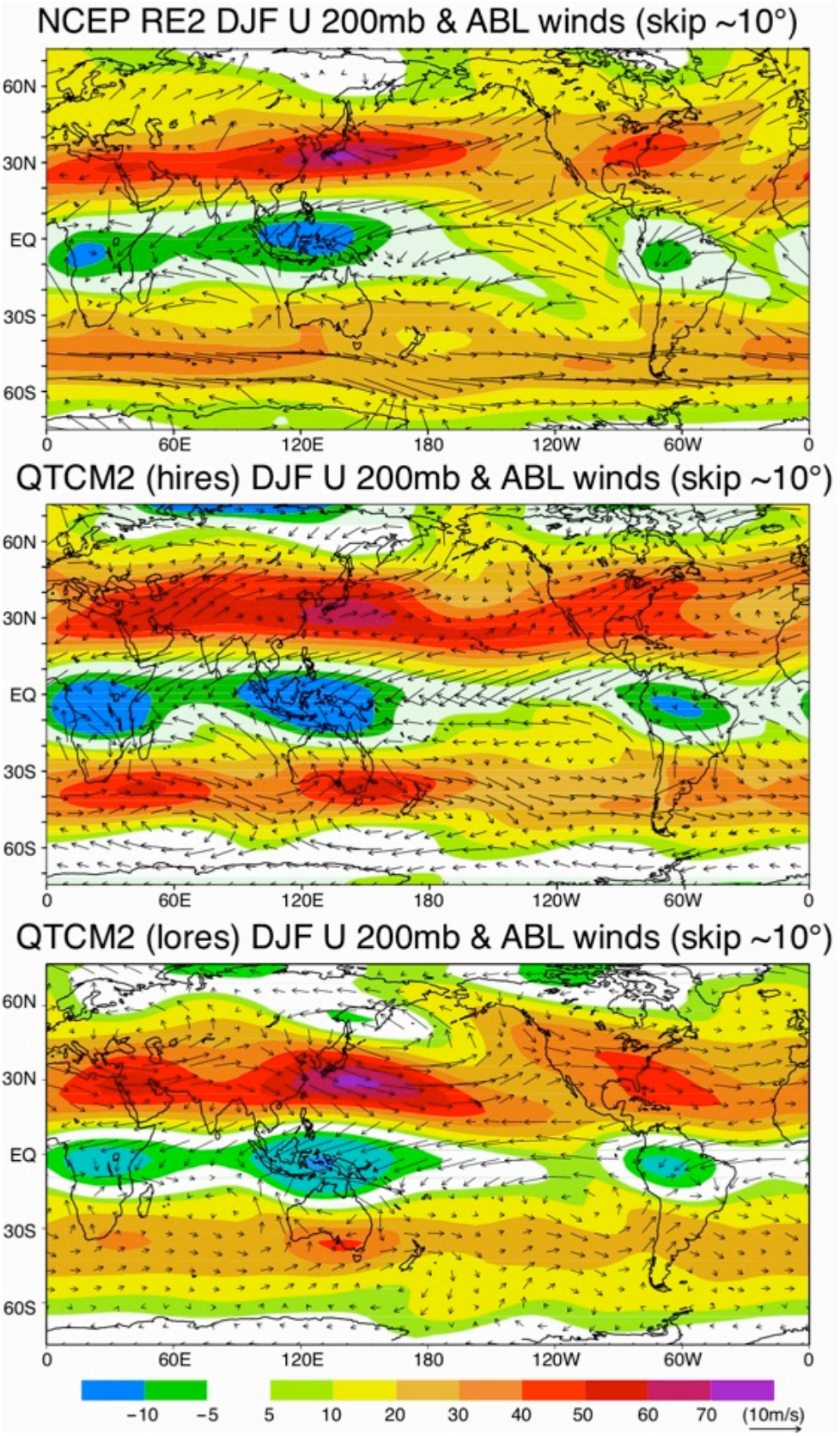
NCEP RE2 DJF U 200mb & ABL winds (skip ~10°)
QTCM2 (hires) DJF U 200mb & ABL winds (skip ~10°)
QTCM2 (lores) DJF U 200mb & ABL winds (skip ~10°)
60N
30N
EQ
30S
60S
0
60E
120E
180
120W
60W
−10
−5
5
10
20
30
40
50
60
70
(10m/s)

836
837

Fig. 6

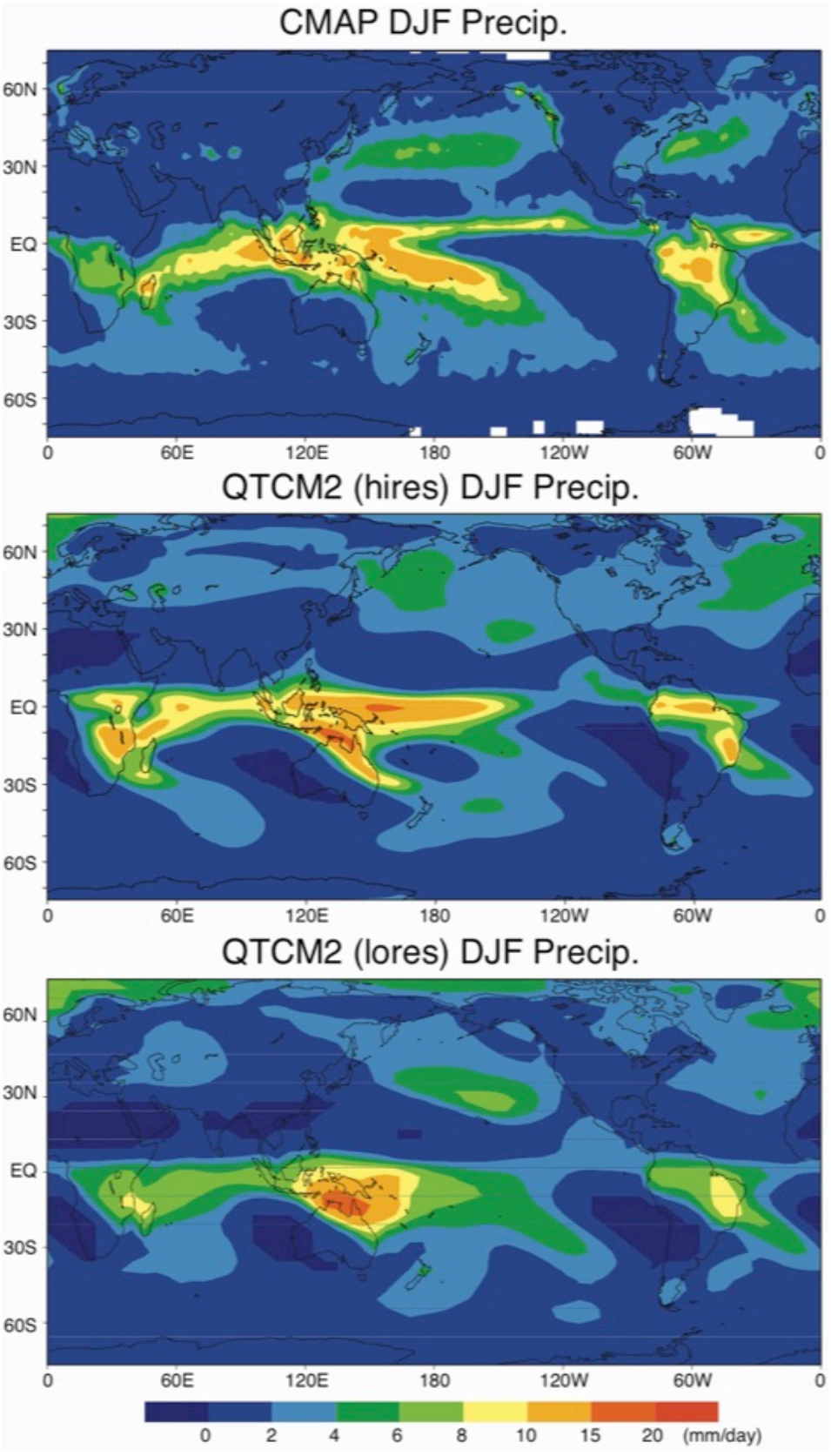
CMAP DJF Precip.
60N
30N
EQ
30S
60S
0
60E
120E
180
120W
60W
0
QTCM2 (hires) DJF Precip.
60N
30N
EQ
30S
60S
0
60E
120E
180
120W
60W
0
QTCM2 (lores) DJF Precip.
60N
30N
EQ
30S
60S
0
60E
120E
180
120W
60W
0
0
2
4
6
8
10
15
20
(mm/day)

838
839

Fig. 7

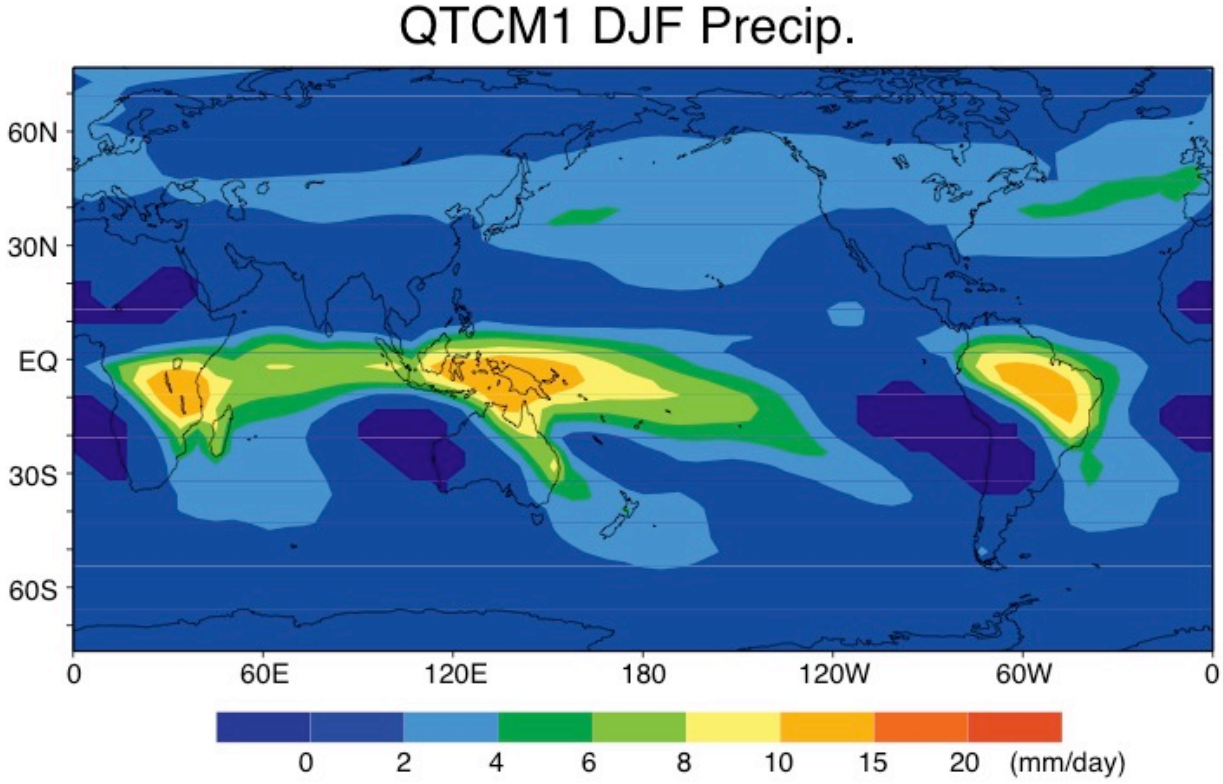
QTCM1 DJF Precip.
60N
30N
EQ
30S
60S
0
60E
120E
180
120W
60W
0
0
2
4
6
8
10
15
20
(mm/day)

840
841

Fig. 8

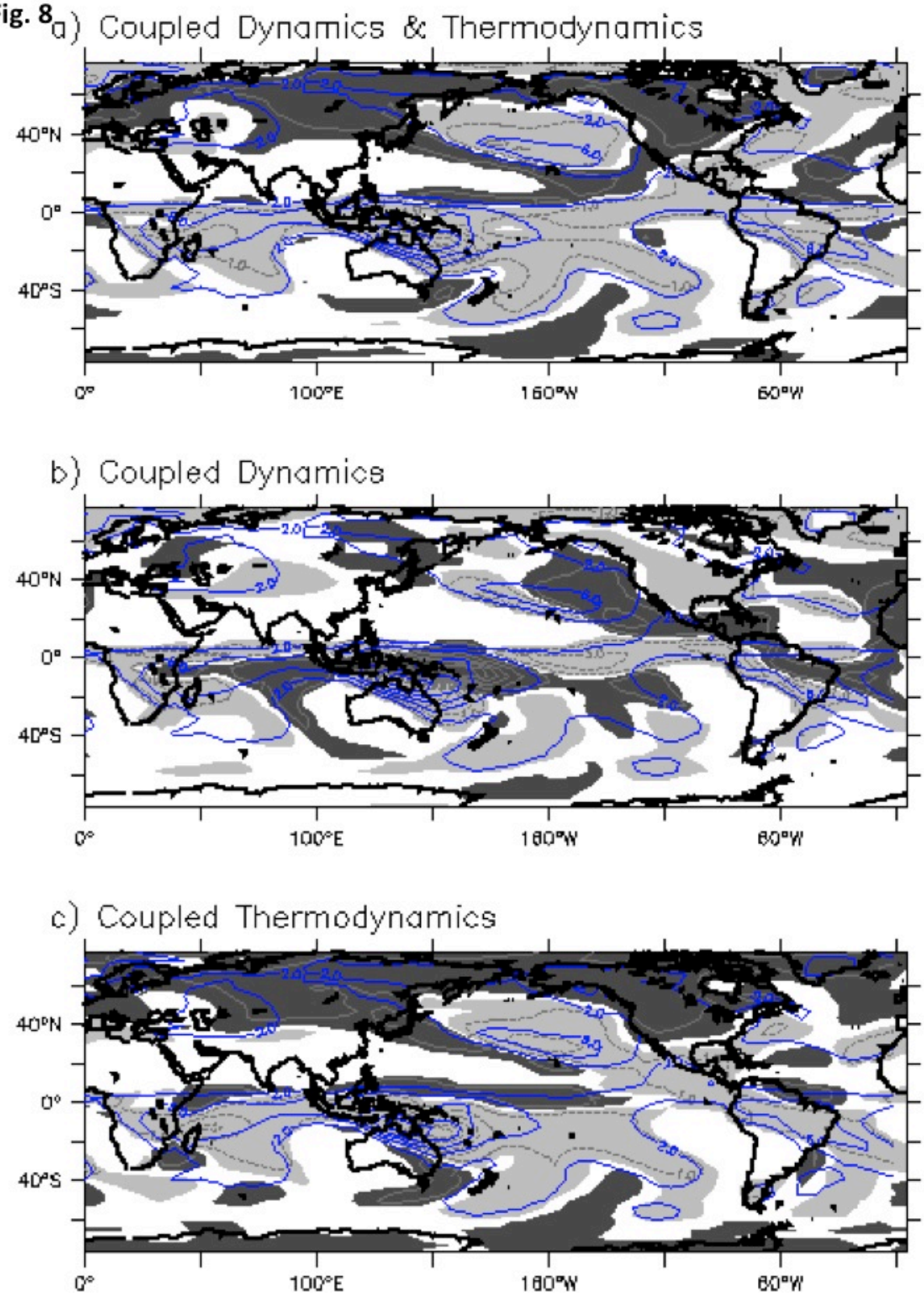
a) Coupled Dynamics & Thermodynamics
40°N
0°
40°S
0°
100°E
160°W
60°W
b) Coupled Dynamics
40°N
0°
40°S
0°
100°E
160°W
60°W
c) Coupled Thermodynamics
40°N
0°
40°S
0°
100°E
160°W
60°W

842
843

Fig. 9

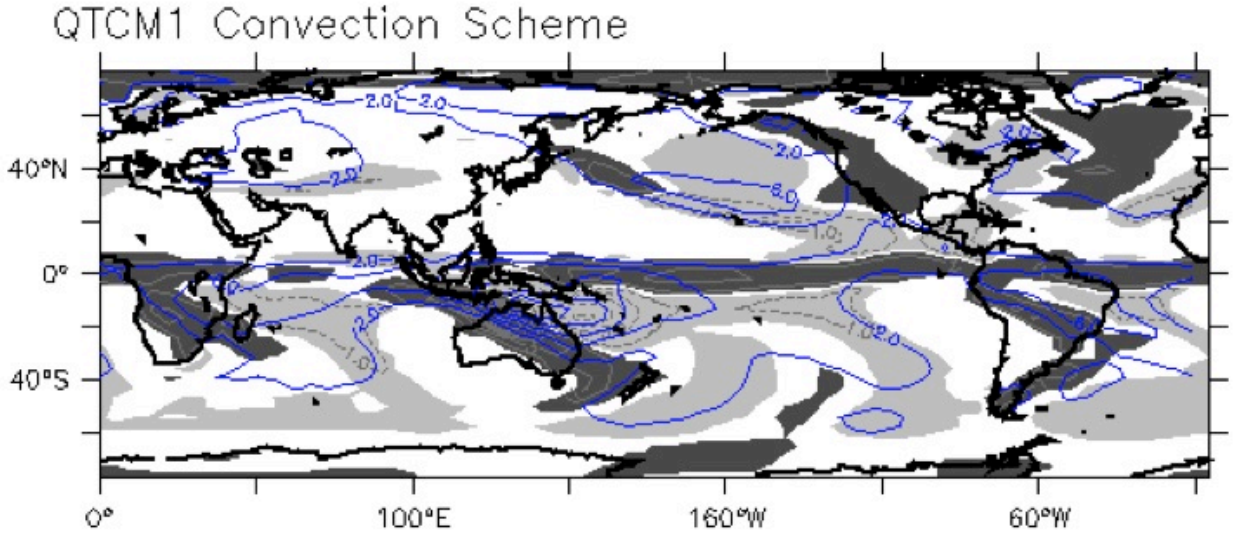

Fig. 10

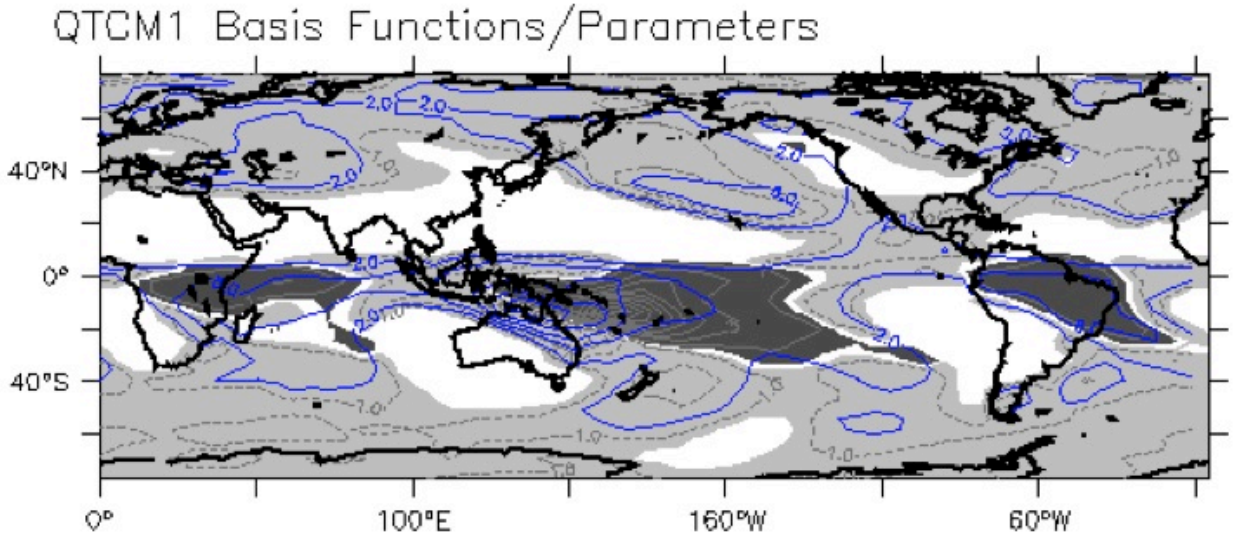

844
845

Fig. 11

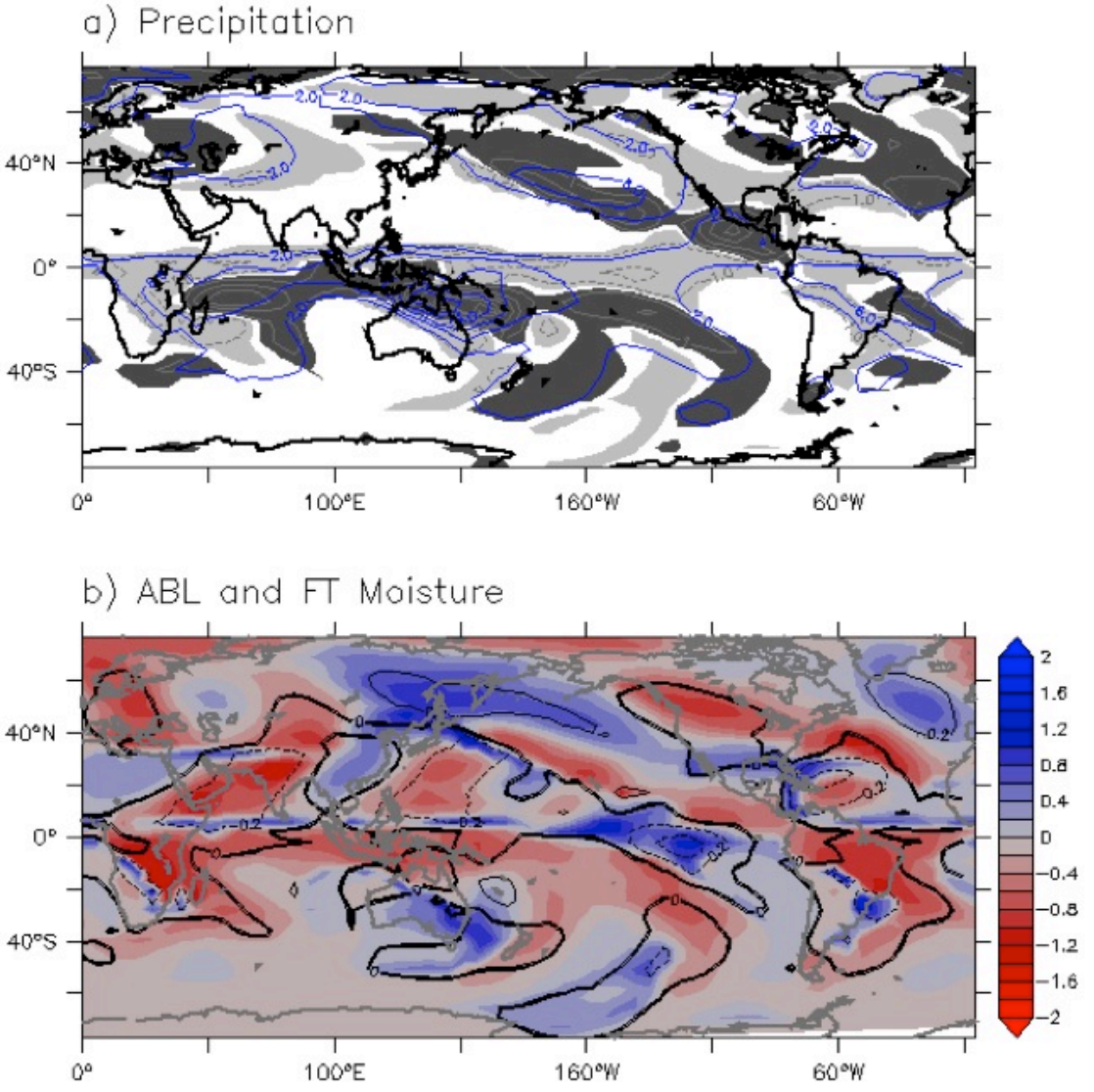

846
847

Fig. 12

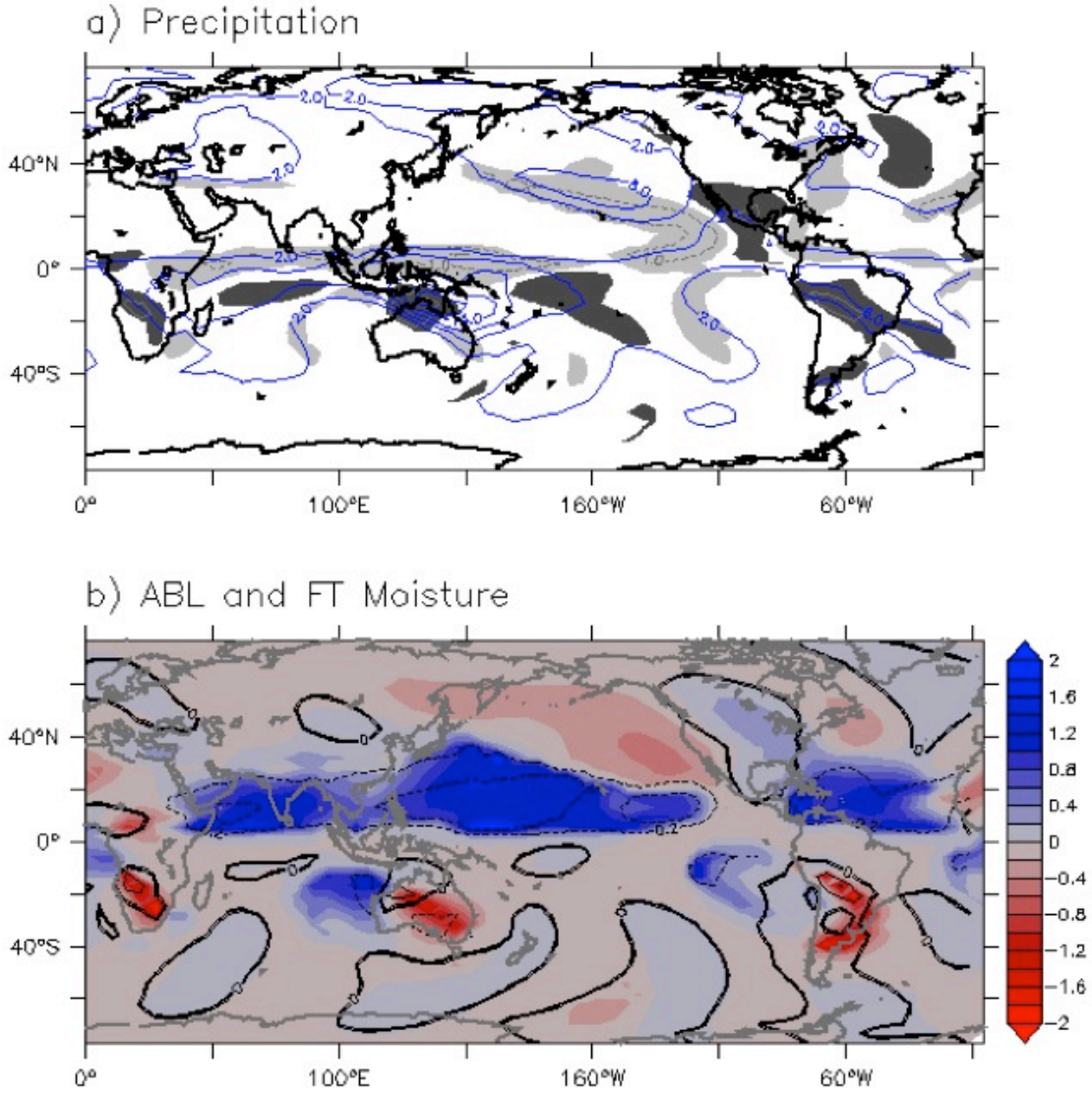

848
849

Fig. 13

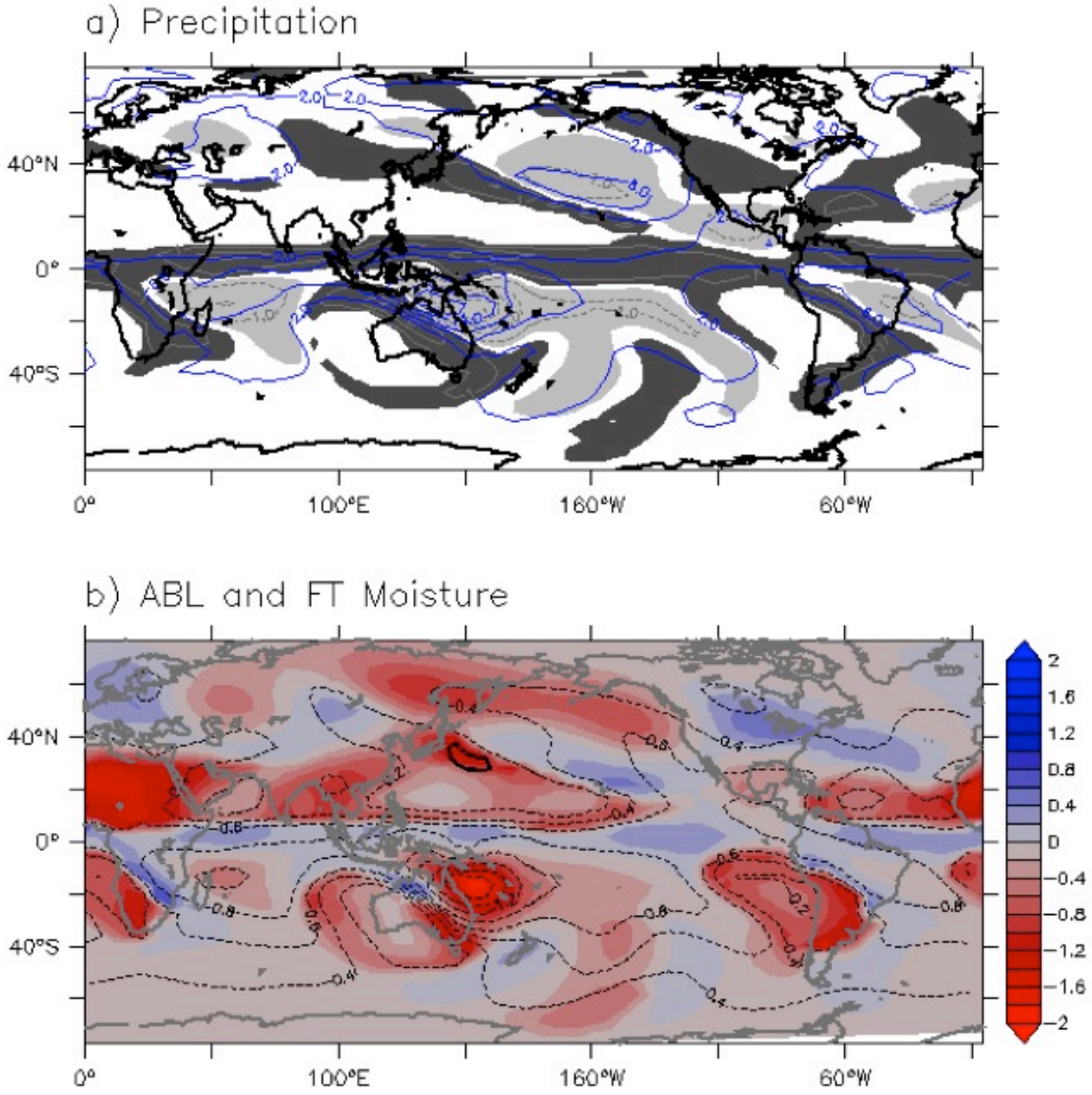

850
851

Fig. 14

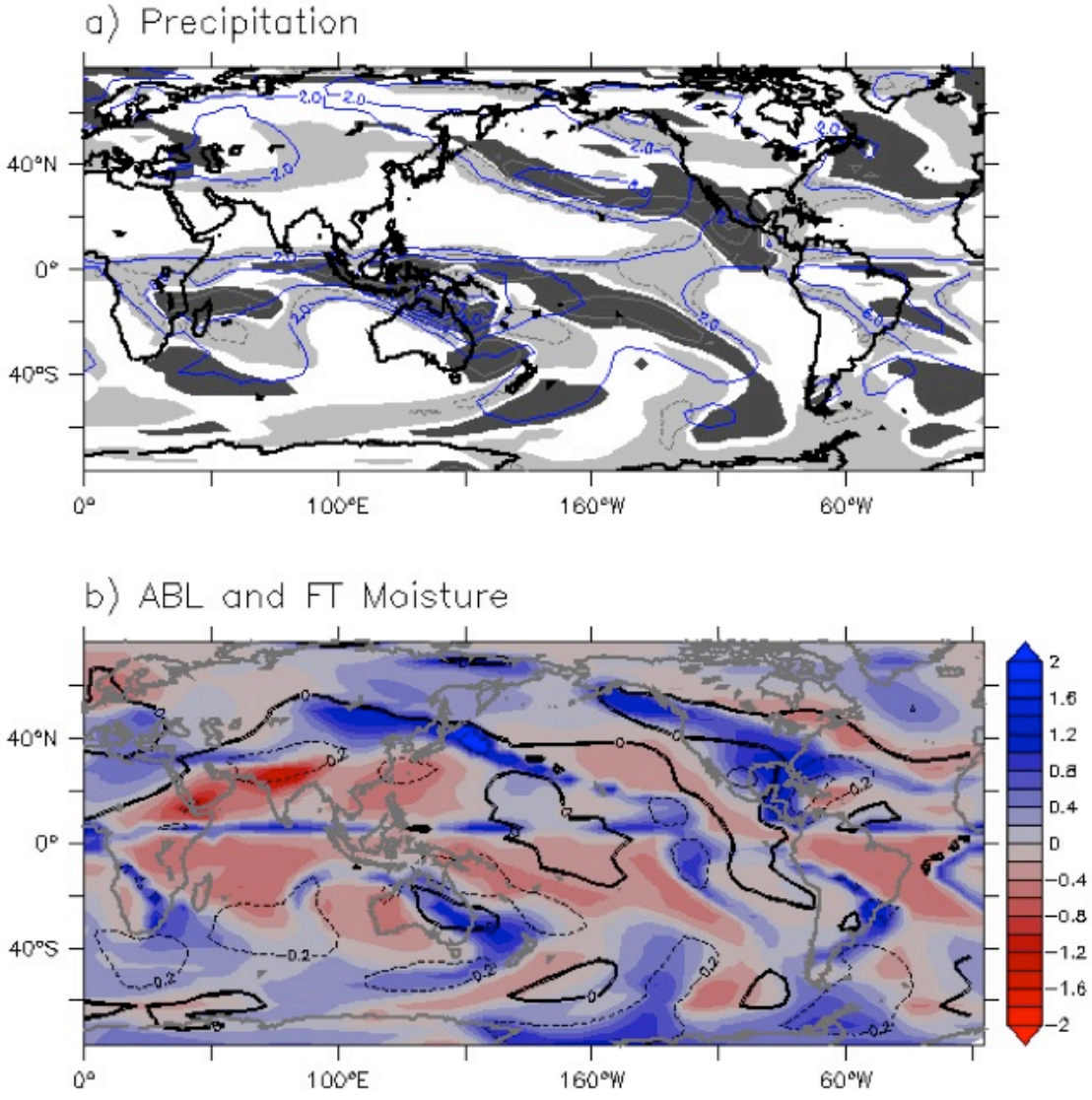
a) Precipitation
40°N
0°
40°S
0°
100°E
160°W
60°W
b) ABL and FT Moisture
40°N
0°
40°S
0°
100°E
160°W
60°W
2
1.6
1.2
0.8
0.4
0
−0.4
−0.8
−1.2
−1.6
−2

852